THE EFFECTS OF THE Mn/Zn RATIO ON THE THERMAL STABILITY OF MnO-ZnO-B_2O_3-SiO_2 GLASS SYSTEM

BY

GARRETT J. VANDER STOUW

A THESIS
SUBMITTED TO THE FACULTY OF

ALFRED UNIVERSITY

IN PARTIAL FULFILLMENT OF THE REQUIREMENTS
FOR THE DEGREE OF

MASTER OF SCIENCE

IN

CERAMIC ENGINEERING

ALFRED, NEW YORK

February, 2020

THE EFFECTS OF THE Mn/Zn RATIO ON THE THERMAL STABILITY OF MnO-ZnO-B_2O_3-SiO_2 GLASS SYSTEM

BY

GARRETT J. VANDER STOUW

M.S. ALFRED UNIVERSITY (2020)

SIGNATURE OF AUTHOR_____

APPROVED BY_____

DR. S.K. SUNDARAM, ADVISOR

_____

DR. STEVEN C. TIDROW, ADVISORY COMMITTEE

_____

DR. ALEXIS G. CLARE, ADVISORY COMMITTEE

_____

Dr. DORIS MÖNCKE, CHAIR, ORAL THESIS DEFENSE

ACCEPTED BY_____

GABRIELLE GAUSTAD, DEAN
KAZUO INAMORI SCHOOL OF ENGINEERING

Alfred University theses are copyright protected and may be used for education or personal research only. Reproduction or distribution in part or whole is prohibited without written permission from the author.

Signature page may be viewed at Scholes Library, New York State College of Ceramics, Alfred University, Alfred, New York.

ACKNOWLEDGMENTS

I would like to acknowledge and express appreciation for the support of: my advisor Dr. S.K. Sundaram for his optimism, understanding, and insight. My committee members Dr. Alexis Clare and Dr. Steven Tidrow, who helped test the limits of my work and suggest ways to solve issues I encountered. I acknowledge the support of the Inamori School of Engineering, the Professors Darren Stohr and Scott Misture, and the Graduate Students Charlie Bellows and Sean Locker. Lastly, I would like to thank my friends and family, who provided endless love and support throughout the graduate school process.

TABLE OF CONTENTS

Page

Acknowledgments ..... *iii*

List of Tables ..... *vi*

List of Figures ..... *viii*

Abstract ..... *xiv*

I. INTRODUCTION **1**

A. Background on MnO Dopant 1

II. EXPERIMENTAL PROCEDURE **2**

A. Sample Preperation 2

B. Characterization 4

1. Thermal Properties *4*

2. Phase Composition *4*

3. Density by Archimedes' Method *5*

III. RESULTS AND DISCUSSION **6**

A. Thermal Properties 7

B. Phase Composition 9

Rietveld Structural Refinement *12*

SEM Imaging and EDS Chemical Analysis *19*

IV. SUMMARY AND CONCLUSIONS **24**

V. FUTURE WORK **25**

VI. REFERENCES **53**

VII. APPENDIX – ADDITIONAL WORK COMPLETED **26**

A. Sample Preparation 26

B. Femtosecond Laser Irradiation and Optical Characterization 27

C. Raman Spectroscopy 38

D. Terahertz Time Domain Spectroscopy 39

E. Additional THz Data Generated 43

Refractive Index *43*

Absorbance *44*

F. DSC-TGA Data 46

1. Temperature Difference *46*
G. XRD SPECTROPSCOPY DATA 47
H. SEM AND EDS DATA 48
Spot Analysis *48*
Additional Images *52*

LIST OF TABLES

Page

Table I: Sample compositions (mol%) of (ZnO,MnO)- B_2O_3- SiO_2 glass 3

Table II: Rietveld structural refinement for post heat-treatment zinc borosilicate glass powder XRD peaks 13

Table III: Rietveld structural refinement for post heat-treatment MnO-doped zinc borosilicate glass powder, of Mn/Zn ratio 0.005:1, XRD peaks 15

Table IV: Rietveld structural refinement for post heat-treatment MnO-doped zinc borosilicate glass powder, of Mn/Zn ratio 0.01:1, XRD peaks 16

Table V: Rietveld structural refinement for post heat-treatment MnO-doped zinc borosilicate glass powder, of Mn/Zn ratio 0.015:1, XRD peaks 18

Table AI: Energy Dispersive Spectroscopy based elemental spot analysis of MnO-doped zinc borosilicate glass powder, of Mn/Zn ratio 0.005:1; location 2, spot 1, post heat-treatment at 875°C 50

Table AII: Energy Dispersive Spectroscopy based elemental spot analysis of MnO-doped zinc borosilicate glass powder, of Mn/Zn ratio 0.005:1; location 2, spot 2, post heat-treatment at 875°C 50

Table AIII: Energy Dispersive Spectroscopy based elemental spot analysis of MnO-doped zinc borosilicate glass powder, of Mn/Zn ratio 0.01:1; location 3, spot 1, post heat-treatment at 875°C 51

Table AIV: Energy Dispersive Spectroscopy based elemental spot analysis of MnO-doped zinc borosilicate glass powder, of Mn/Zn ratio 0.005:1; location 2, spot 2, post heat-treatment at 875°C 51

Table AV: Energy Dispersive Spectroscopy based elemental spot analysis of MnO-doped zinc borosilicate glass powder, of Mn/Zn ratio 0.01:1; location 3,upper right spot 1, post heat-treatment at 875°C 52

Table AVI: Energy Dispersive Spectroscopy based elemental spot analysis of MnO-doped zinc borosilicate glass powder, of Mn/Zn ratio 0.015:1; location 2, spot 3, post heat-treatment at 951°C with a ramp rate of 10°C/min 52

Table AVII: Energy Dispersive Spectroscopy based elemental spot analysis of MnO-doped zinc borosilicate glass powder, of Mn/Zn ratio 0.015:1; location 2, spot 4, post heat-treatment at 951°C with a ramp rate of 10°C/min 53

Table AVIII: Energy Dispersive Spectroscopy based elemental spot analysis of MnO-doped zinc borosilicate glass powder, of Mn/Zn ratio 0.015:1; location 2, spot 5, post heat-treatment at 951°C with a ramp rate of 10°C/min 53

LIST OF FIGURES

Page

Figure 1: (MnO,ZnO)B_2O_3-SiO glass samples with and without B_2O_3 phase separation caused by annealing at 500°C and 620°C (a,b) 6

Figure 2: DSC curves of MnO-doped zinc borosilicate glass powder, (a) at a 20°C/min heat rate and (b) a 10°C/min heat rate. T_g, T_p, and T_m temperatures are noted. 7

Figure 3: XRD Peaks of MnO-doped zinc borosilicate glass powder heat-treated at 951°C via 10°C/min ramp and mixed with high purity Si standard material to account for instrument error in peak shift..... 9

Figure 4: XRD peaks of MnO-doped zinc borosilicate glass powder, of Mn:Zn ratio 0.015:1 (0.82 MnO mol%), post heat-treatment to 875°C at 20°C/min and 951°C at 10°C/min. 10

Figure 5: XRD peaks of MnO-doped zinc borosilicate glass powder, (a) after heat-treating at 875°C and (b) after heat-treating at approximately 955°C with a 10°C/min heat rate, where the Mn:Zn ratios are 0, 0.005, 0.01, and 0.015 for compositions of MnO mol% 0 – 0.82 respectively. 11

Figure 6: Mn-doped zinc borosilicate glass powder XRD peaks for particle size comparison. 11

Figure 7: Rietveld structural refinement for post heat-treatment, held at 875°C, zinc borosilicate glass powder XRD peaks. Analyzed in comparison to $Zn_4O(BO_2)_6$ (PDF 01-076-0917) and willemite: Zn_2SiO_4 (PDF 04-008-0329) phases. 14

Figure 8: Rietveld structural refinement for post heat-treatment, ramped to and held at 955°C at a rate of 10°C/min, zinc borosilicate glass powder XRD peaks. Analyzed in comparison to $Zn_4O(BO_2)_6$ (PDF 01-076-0917) and willemite: Zn_2SiO_4 (PDF 04-008-0329) phases. 14

Figure 9: Rietveld structural refinement for post heat-treatment, held at 875°C, MnO-doped zinc borosilicate glass powder, of Mn:Zn ratio 0.005:1, XRD peaks. Analyzed in comparison to $Zn_4O(BO_2)_6$ (PDF 01-076-0917) and willemite: Zn_2SiO_4 (PDF 04-008-0329) phases. 15

Figure 10: Rietveld structural refinement for post heat-treatment, ramped to and held at 955°C at a rate of 10°C/min, MnO-doped zinc borosilicate glass powder, of Mn:Zn ratio 0.005:1, XRD peaks. Analyzed in comparison to $Zn_4O(BO_2)_6$ (PDF 01-076-0917) and willemite: Zn_2SiO_4 (PDF 04-008-0329) phases. 16

Figure 11: Rietveld structural refinement for post heat-treatment, held at 875°C, MnO-doped zinc borosilicate glass powder, of Mn:Zn ratio 0.01:1, XRD peaks. Analyzed in comparison to $Zn_4O(BO_2)_6$ (PDF 01-076-0917) and willemite: Zn_2SiO_4 (PDF 04-008-0329) phases. 17

Figure 12: Rietveld structural refinement for post heat-treatment, ramped to and held at 955°C at a rate of 10°C/min, MnO-doped zinc borosilicate glass powder, of Mn:Zn ratio 0.01:1, XRD peaks. Analyzed in comparison to $Zn_4O(BO_2)_6$ (PDF 01-076-0917) and willemite: Zn_2SiO_4 (PDF 04-008-0329) phases. 17

Figure 13: Rietveld structural refinement for post heat-treatment, held at 875°C, MnO-doped zinc borosilicate glass powder, of Mn:Zn ratio 0.015:1, XRD peaks. Analyzed in comparison to $Zn_4O(BO_2)_6$ (PDF 01-076-0917) and willemite: Zn_2SiO_4 (PDF 04-008-0329) phases. 18

Figure 14: Rietveld structural refinement for post heat-treatment, ramped to and held at 955°C at a rate of 10°C/min, MnO-doped zinc borosilicate glass powder, of Mn:Zn ratio 0.015:1, XRD peaks. Analyzed in comparison to $Zn_4O(BO_2)_6$ (PDF 01-076-0917) and willemite: Zn_2SiO_4 (PDF 04-008-0329) phases. 19

Figure 15: EDS elemental mapping of zinc borosilicate glass powder heat-treated at 875°C, Au-sputter coated, and utilizing back scattering electrons. 20

Figure 16: EDS elemental mapping of MnO-doped zinc borosilicate glass powder, of Mn:Zn ratio 0.005:1 for composition of MnO mol% 0.27, heat-treated at 875°C, Au-sputter coated, and utilizing back scattering electrons. Map 1 20

Figure 17: EDS elemental mapping of MnO-doped zinc borosilicate glass powder, of Mn:Zn ratio 0.005:1 for composition of MnO mol% 0.27, heat-treated at 875°C, Au-sputter coated, and utilizing back scattering electrons. Map 2 21

Figure 18: EDS elemental mapping of MnO-doped zinc borosilicate glass powder, of Mn:Zn ratio 0.005:1 for composition of MnO mol% 0.27, heat-treated at 875°C, Au-sputter coated, and utilizing back scattering electrons. Map 3 21

Figure 19: EDS elemental mapping of MnO-doped zinc borosilicate glass powder, of Mn:Zn ratio 0.015:1 for composition of MnO mol% 0.82, heat-treated at 875°C, Au-sputter coated, and utilizing back scattering electrons..... 22

Figure 20: EDS elemental mapping of MnO-doped zinc borosilicate glass powder heat-treated to 955°C at a rate of 10°C/min, Au-sputter coated, and utilizing back scattering electrons. 23

Figure A1: Cut, ground, and polished samples of MnO-doped zinc borosilicate glass, of Mn/Zn ratios 0, 0.005, 0.01, and 0.015 for compositions of MnO mol% 0 – 0.82 respectively(a-d). 28

Figure A2: MnO-doped zinc borosilicate glass powder, of Mn/Zn ratios 0:1 and 0.015:1(a) and 0.01:1 and 0.015(b) for compositions of MnO mol% 0.55 and 0.82 respectively under UV light. Post heat-treatment at 10C/min to ≈ 955°C. Exhibiting the 0 photoluminescence, 0:1 Mn:Zn, reddish orange photoluminescence generated via glass containing Mn^{3+}, 0:01:1 Mn:Zn, and the yellow-green produced via ceramic containing Mn^{2+}. 28

Figure A3: Cut and polished MnO-doped zinc borosilicate glass, of Mn/Zn ratios 0, 0.005, 0.01, and 0.015 for compositions of MnO mol% 0 – 0.82 respectively, pre and post laser application, 1.5 = 1 mm/s and 1 = 0.5 mm/s rastering speed for laser application. Shown in both natural light and UV light. 30

Figure A4: MnO-doped zinc borosilicate glass powder, of Mn/Zn ratios 0, 0.005, 0.01, and 0.015 for compositions of MnO mol% 0 – 0.82 respectively, after heat-treating at 10°C/min to 952,953,954, 955°C respectively..... 11

Figure A5: Fluorescence Spectroscopy peaks of MnO-doped zinc borosilicate glass powder, of Mn/Zn ratios 0, 0.005, 0.01, and 0.015 for compositions of MnO mol% 0 – 0.82 respectively(top) and of Mn/Zn ratios 0.005, 0.01, and 0.015, for compositions of MnO mol% 0.27 – 0.82, utilizing Mn/Zn ratios 0:1 as background noise(bottom). 3211

Figure A6: Cut and polished MnO-doped zinc borosilicate glass, of Mn/Zn ratio 0.015:1, post femtosecond laser application of 0.5 mm/s rastering speed and ≈ 7.8 W, examined via backscattering electron SEM and exhibiting thin film scribing..... 35

Figure A7: Cut and polished zinc borosilicate glass, post femtosecond laser application of 0.5 mm/s rastering speed and ≈ 7.8 W, examined via backscattering electron SEM and exhibiting either thin film scribing or ultrafast annealing..... 36

Figure A8: Cut and polished MnO-doped zinc borosilicate glass, of Mn/Zn ratio 0.01:1, post femtosecond laser application of 1 mm/s rastering speed and ≈ 7.8 W, examined via backscattering electron SEM and exhibiting structures similar to ns ablation. 37

Figure A9: Cut and polished zinc borosilicate glass, post femtosecond laser application of 1 mm/s rastering speed and ≈ 7.8 W, examined via backscattering electron SEM and exhibiting ZnO nanowire, potentially Mn doped, in a silicate phase..... 39

Figure A10: Raman peaks of MnO-doped zinc borosilicate glass, of Mn/Zn ratios 0, 0.005, 0.01, and 0.015 for compositions of MnO mol% 0 – 0.82 respectively (a-d) exhibiting the effects of laser application at rastering speeds 1mm/s and 0.5 mm/s. 40

Figure A11: Refractive Index(a) and Absorbance(b) peaks of MnO-doped zinc borosilicate glass powder, of Mn/Zn ratios 0, 0.005, 0.01, and 0.015 for compositions of MnO mol% 0 – 0.82 respectively..... 42

Figure A12: 0.8 THz Comparison RI (a) and Absorbance (b) of MnO-doped zinc borosilicate glass powder, of Mn/Zn ratios 0, 0.005, 0.01, and 0.015 for compositions of MnO mol% 0 – 0.82 respectively..... 44

Figure A13: Refractive index of MnO-doped zinc borosilicate glass, of Mn/Zn ratios 0, 0.005, 0.01, and 0.015 for compositions of MnO mol% 0 – 0.82 respectively (a-d) measured via THz Time-Domain. 45

Figure A14: Absorbance of MnO-doped zinc borosilicate glass, of Mn/Zn ratios 0, 0.005, 0.01, and 0.015 for compositions of MnO mol% 0 – 0.82 respectively (a-d) measured via THz Time-Domain. 46

Figure A15: Dielectric Constants Real(a) and Imaginary(b) of MnO-doped zinc borosilicate glass, of Mn/Zn ratios 0, 0.005, 0.01, and 0.015 for compositions of MnO mol% 0 – 0.82 respectively..... 47

Figure A16: Exo- and endothermic temperature difference of MnO-doped zinc borosilicate glass, of Mn/Zn ratios 0, 0.005, 0.01, and 0.015 for compositions of MnO mol% 0 – 0.82 respectively (a-d) vs temperature, measured via differential scanning calorimetry. Samples were measured at a 20°C/min heating-rate and a 10°C/min heating-rate. 48

Figure A17: XRD peaks of MnO-doped zinc borosilicate glass powder, of Mn/Zn ratios 0(a) and 0.005(b), of compositions MnO mol% 0 and 0.27 respectively, comparison between heat-treatment to 875°C at a rate of 20°C/min and to ≈ 955°C/min at a rate of 10°C/min. 49

Figure A18: Energy Dispersive Spectroscopy based elemental spot analysis of MnO-doped zinc borosilicate glass powder, of Mn/Zn ratio 0.005:1; location 2, spot 1, post heat-treatment at 875°C. 50

Figure A19: Energy Dispersive Spectroscopy based elemental spot analysis of MnO-doped zinc borosilicate glass powder, of Mn/Zn ratio 0.005:1; location 2, spot 2, post heat-treatment at 875°C. 50

Figure A20: Energy Dispersive Spectroscopy based elemental spot analysis of MnO-doped zinc borosilicate glass powder, of Mn/Zn ratio 0.01:1; location 3, spot 1, post heat-treatment at 875°C. 51

Figure A21: Energy Dispersive Spectroscopy based elemental spot analysis of MnO-doped zinc borosilicate glass powder, of Mn/Zn ratio 0.01:1; location 3, lower left spot 1, post heat-treatment at 875°C. 51

Figure A22: Energy Dispersive Spectroscopy based elemental spot analysis of MnO-doped zinc borosilicate glass powder, of Mn/Zn ratio 0.01:1; location 3,upper right spot 1, post heat-treatment at 875°C. 52

Figure A23: Energy Dispersive Spectroscopy based elemental spot analysis of MnO-doped zinc borosilicate glass powder, of Mn/Zn ratio 0.015:1; location 2, spot 3, post heat-treatment at 951°C with a ramp rate of 10°C/min. 52

Figure A24: Energy Dispersive Spectroscopy based elemental spot analysis of MnO-doped zinc borosilicate glass powder, of Mn/Zn ratio 0.015:1; location 2, spot 4, post heat-treatment at 951°C with a ramp rate of 10°C/min. 53

Figure A25: Energy Dispersive Spectroscopy based elemental spot analysis of MnO-doped zinc borosilicate glass powder, of Mn/Zn ratio 0.015:1; location 2, spot 5, post heat-treatment at 951°C with a ramp rate of 10°C/min. 53

Figure A26: Scanning electron microscopic imaging of MnO-doped zinc borosilicate glass powder, of Mn/Zn ratios 0.005:1(a) and 0.01:1(b) of compositions MnO mol% 0.27 and 0.55 respectively after heat-treatment at 875°C. 54

Figure A27: SEM imaging of Energy Dispersive Spectroscopy based elemental spot analysis of MnO-doped zinc borosilicate glass powder, of Mn/Zn ratio 0.015:1 of composition MnO mol% 0.82 after heat-treatment at 951° C with a ramp rate of 10°C/min. 54

ABSTRACT

The focus of this thesis is a relatively overlooked subset of the MnO-doped zinc borosilicate glass system with a goal of investigating the effects of MnO-doping on the thermal stability of crystallite phase formation in the system. A glass system of general composition $55ZnO\text{-}20B_2O_3\text{-}25SiO_2$ with added MnO dopant, which replaces Zn modifier locations with Mn, of ratios 0, 0.005, 0.01, and 0.015 MnO:ZnO were prepared, via. batch melting at 1550°C for 1.5 h. The glasses were characterized using differential scanning calorimetry (DSC), thermogravimetric analysis (TGA), x-ray diffraction (XRD), scanning electron microscopy (SEM), energy-dispersive spectrometry (EDS). Thermal analysis, followed by detailed XRD and Rietveld structural refinement, reveal the formation of zinc borate ($Zn_4O(BO_2)_6$), willemite (Zn_2SiO_4), and manganese zinc silicate ($(ZnMn)SiO_4$) crystallites after heat-treatment at 875°C for 4 h and no zinc borate crystallite in samples heated to ≈ 955°C at a ramp rate of 10°C/min and held for 4 h. Microstructure and elemental maps confirmed that the zinc borate had become an integral part of a glass phase in the resulting glass-ceramic samples. Low MnO-content influences the formation of the boron-containing glass phase. When heat-treated at the transition point between two crystalline maxima, 875°C, samples exhibited a variety of structures as glass-ceramics of zinc borate and willemite/(Mn,Zn) silicate crystalline phases regardless of Mn:Zn ratio. Samples heat-treated to the T_m, ≈ 955°C, at a rate of 10°C/min showed nucleation of SiO_2 inclusions and willemite / manganese zinc silicate crystallites in a zinc borosilicate glass matrix, with increasing zinc borosilicate Mn:Zn ratio.

I. INTRODUCTION

Zinc borosilicate glasses are known for their thermal shock resistance, high elastic moduli, chemical durability, low level of optical absorbance, and the piezoelectric properties of ZnO.[1-2] In recent years, there has been an increase in interest and documentation of the fluorescent behavior of zinc borosilicate glasses through the formation of zincite, a rarer mineral form of ZnO, and willemite, Zn_2SiO_4, crystalline phases as ultraviolet (UV) emission centers.[3-5] The glasses need to be crystallized via heat-treatment, or other methods, and converted into a glass-ceramic to generate these phases, bringing the added benefits of strength, heat resistance, low production expense, and higher thermal shock resistance at the cost of some optical clarity.[4] These glass-ceramics have recently been studied for use in optical devices such as high energy detectors.[3-5]

In this thesis, we chose the ternary ZnO-B_2O_3-SiO_2 system as a base system to study the effects of controlled post processing thermal treatment. In the chosen system, SiO_2 and B_2O_3 act as network formers. B_2O_3 additionally functions as a flux, lowering the melting point of the glass. Boron atoms have been found[6] to be present in the cubic crystalline zinc borate in four-fold coordination with oxygen, and transition to three-fold coordination during melting. Zinc oxide, responsible for forming non-bridging oxygens (NBOs) within the structure to try to induce a greater degree of crystallization, is present at the maximum solubility level in this system, ≈ 55 mol%, as one of two network modifiers, the other being the dopant MnO.[4]

A. Background on MnO Dopant

MnO-doped ZnO-B_2O_3-SiO_2 glass and glass-ceramic systems have been a topic of interest due to their potential and inherent ferromagnetic, electrical, and photoluminescent properties.[2,6-9] The Mn^{2+} in MnO, the chosen dopant for this thesis, acts as a network modifier within the glass structure similar to the Zn^{2+} from ZnO which possesses a similar radius of approximately 0.6Å. Mn^{2+} is a paramagnetic ion that will, in a lattice with Zn^{2+} ions, substitute for Zn^{2+} sites or otherwise occupy interstitial sites in the glass structure.[6] In glass systems containing MnO, Mn^{2+} and Mn^{3+} are expected to be observed, while Mn^{4+}

is not expected to be observed due to specific valance conditions within the system.[2] The Mn^{3+} formation is due to oxidation during the melt processes, however it has been shown that the ratio of Mn^{3+} ions to overall expected Mn ionic content, of Mn^{2+} and Mn^{3+} ions, will not exceed 0.03 in MnO-doped amorphous systems.[2,6] The generation of Mn^{3+} leads to a color composition in doped zinc borosilicate glasses that ranges from light pink to brown.[6] Mn^{2+} doped zinc borosilicate glasses are shown in past studies to emit green luminescence, reddish-orange photoluminescence under UV light due to the willemite-like phases formed by four-fold coordinated Mn^{2+}/Zn^{2+} glass structure modifiers, and yellowish/greenish photoluminescence as part of a glass-ceramic.[6,9] A reddish, long lasting phosphoresce has also been observed in the glasses, which becomes a yellowish and/or greenish phosphorescence after undergoing heat-treatment to form glass-ceramics.[9]

In recent years, there have been a selection of papers published on the potential electrical and optical applications of unique compositions of the MnO-doped ZnO-B_2O_3-SiO_2 system.[2,6-9] While the Mn/Zn ratio has been noted in other studies, few utilized it as the primary form of composition alteration. Thus, it would be beneficial to study how this glass system behaves in relation to the Mn/Zn mol% ratio of the glass system. We present our data, observations, and interpretations on potential changes in thermal and structural properties of MnO-doped ZnO-B_2O_3-SiO_2 system investigated via heat-treatment at key transitional temperatures of the system.

II. EXPERIMENTAL PROCEDURE

A. Sample Preperation

Glass samples were synthesized using high-purity ZnO, $MnCO_3$, H_3BO_3, and SiO_2 powder precursors (Fisher Chemical, Alfa Aesar) in a platinum crucible. Four target glass compositions were chosen in the MnO-doped ZnO-B_2O_3-SiO_2 system where the Mn/Zn mol% ratio is 0, 0.005, 0.01, and 0.015 and MnO mol% of 0, 0.27, 0.55, and 0.82 respectively. To reduce the risk of phase separation experienced in preliminary trials and support sample homogeneity, the samples were processed following a consistent mass of 7g batches of compositions as shown in Table 1. The batches were melted in a furnace at 1550°C and held at temperature for 1.5 h. After melting, the samples were poured onto a

graphite plate mold to reduce contamination and then transferred to an annealing furnace to hold at 500°C for 1 h, chosen after brief experimentation with annealing temperatures, followed by cooling down to room temperature via unaided cooling.

Table I: Sample compositions (mol% ±0.005) of (ZnO,MnO)- B_2O_3- SiO_2 glass

Composition	**ZnO**	**B_2O_3**	**SiO_2**	**MnO**
1	55.00	20.00	25.00	0.00
2	54.85	19.95	24.93	0.27
3	54.70	19.89	24.86	0.55
4	54.55	19.84	24.80	0.82

B. Characterization

1. Thermal Properties

Glass pieces produced were ground to obtain 20-50 mg of < 250 μm powder in preparation for characterization using differential scanning calorimetry-thermogravimetric analysis (DSC-TGA, SDT Q600, TA Instruments) to determine glass transition and other transition temperatures of the glasses. Powder samples were heated to 1300°C in Pt crucibles to maintain purity and maintain crucible integrity during the process. A reference material of alumina (A-10, Almatis) was used for thermal analysis. The samples were heated at rates of 20°C/min and 10°C/min and cooled with an airflow of 100mL/min.

2. Phase Composition

Based on DSC-TGA data, powdered samples were heat-treated for 4 hours at ≈ 954°C, at a ramp rate of 10°C/min; and at 875°C, at a ramp rate as close to 20°C/min as possible given the limitations of the annealing kilns available. Crystal nucleation and transitional growth events were observed at both treatment temperatures. The samples were heat-treated in a Pt crucible to avoid contamination and allow for easy recovery of the crystallized samples. The crystallized powders were then reground to maintain sample homogeneity for x-ray powder diffraction (XRD, D2 Phasor, Bruker). The XRD scan was performed using a 5.8° opening sensor, Cu tube, and generator set to 30 KV and 10 mA, over the range of 10°-80°2θ with a step size of 0.03°, and a count time of 576 s/step. The XRD patterns obtained were analyzed and fit to existing material PDFs using the program Diffrac4.3. Scanning electron microscopy (SEM, SM-7800F Field Emission Scanning Electron Microscope, JEOL) with backscatter electron imaging was used to avoid the fluorescence caused by high-energy application to Mn-doped materials. Additionally, energy dispersive spectroscopy (EDS, EDAX) driven chemical point analysis was completed for sample imaging and spot compositional analysis using texture and elemental analytical microscopy (TEAM) software. The powdered and heat-treated samples were attached to the sample holders with carbon tape, for a consistent background element, and sputter coated with gold to avoid charging.

3. Density by Archimedes' Method

The density (ρ) of 7g samples of MnO-doped zinc borosilicate glass, with Mn/Zn ratios 0:1, 0.005:1, 0.01:1, and 0.015, were found for comparison to known density values for Mn-doped zinc borosilicate glass, utilizing the Archimedes' method. Mass (m) was determined with a gram balance, sample volume (V) was determined via water displacement measurement using the equation: $\rho=m/V$.

III. RESULTS AND DISCUSSION

The MnO-ZnO-B_2O_3-SiO_2 glass samples, after annealing, were visibly clear glasses with varying intensities of brownish pink coloration that, as expected, increased in coloration with the concentration of MnO and the resulting Mn^{3+} ions that formed via oxidation. Samples consistently show slight opalescent striations radiating from a singular location on the surface of the samples. In correlation with the findings of Ehrt this is understood to be the formation of a thin B_2O_3 phase on portions of the sample surface.[6] Although difficult to achieve, zinc borate glasses have been shown to separate into an opalescent B_2O_3 phase, due to the low number of crystallites, and a clear ZnO-B_2O_3 phase, due to an immiscibility gap that occurs when ZnO < 50% mol and the melt temperature > 982°C.[6] The phase separation is incomplete in the samples due to the ≈ 55 mol% ZnO content. It was found when preparing samples that an annealing temperature of 600-630°C led to higher degrees of a liquid-liquid phase separation, as seen in Figure 1. XRD data shows phase separation into an opalescent borate phase and a clear zinc borosilicate phase, as reported for similar compositions by Ehrt[6], where the opalescent borate phase was found to have stronger crystallites at the surface than in the general volume of the sample.[6]

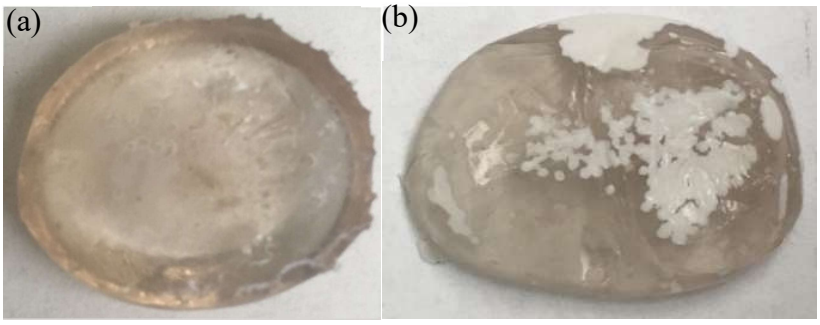

Figure 1: (MnO,ZnO)B_2O_3-SiO glass samples with and without B_2O_3 phase separation caused by annealing at (a) 500°C and (b) 620°C

The density of the glass compositions produced were determined for MnO-doped zinc borosilicate glass of Mn:Zn ratios 0, 0.005, 0.01, and 0.015 as 3.061, 2.576, 2.549, and 2.745 ± 0.05 g/cm^3, respectively. The Archimedes method was used for the measurements. The density values measured were comparable, although they tended to be slightly lower than the values of zinc borosilicate and manganese borosilicate reported in the literature by varying degrees per source.[2,4,6,8,13]

A. Thermal Properties

DSC observations indicate an initial endothermic valley that occurs consistently at an onset temperature of 594-604°C, representing the glass transition temperature (T_g) of the glass at both 20°C/min and 10°C/min heat rates respectively, shown in Figure 2. Samples heat-treated at 20°C/min, unlike those heat-treated at 10°C/min, exhibit decreasing T_g in samples containing MnO dopant content. The temperatures of maximum crystallization (T_p) can be identified, using the exothermic nature of crystallization, as the center of exothermic peaks in the DSC curve, assuming the peaks are of similar width. The compositions at a 20°C/min heating rate show primary T_p from 824-826°C with MnO-doped zinc borosilicate glass of Mn:Zn ratios 0.005, 0.01, and 0.015 producing a secondary value ≈ 934°C. These crystal maxima represent the formation and dissolution of zinc borate and manganese zinc silicate / willemite respectively. This creates a point of interest in the endothermic valley between the T_p, at ≈

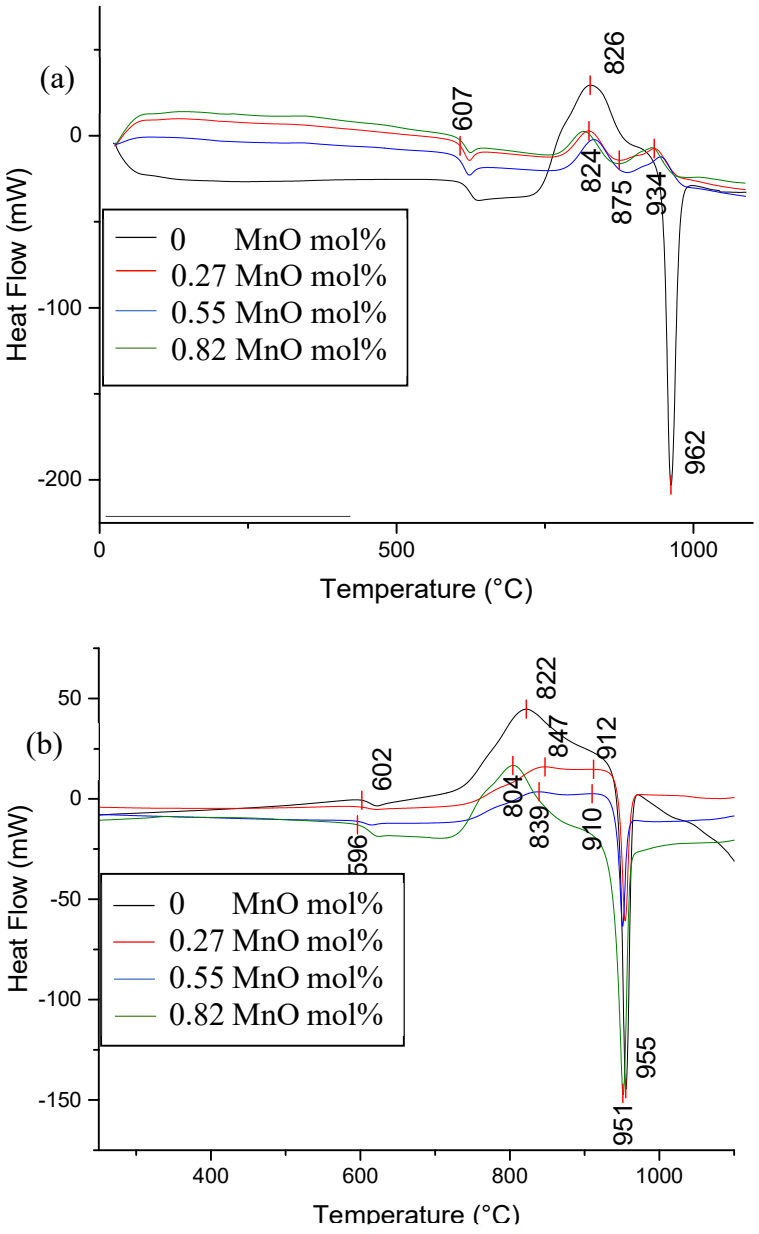

Figure 2: DSC curves of MnO-doped zinc borosilicate glass powder, (a) at a 20°C/min heat rate and (b) a 10°C/min heat rate. T_g, T_p, and T_m temperatures are noted.

875°C, where the crystallites formed by one crystal maxima have mostly subsided into the melt and the crystallites of the next crystal maxima are starting to nucleate. This point will be referred to as the crystalline transition temperature (T_{ct}). The compositions at a 10°C/min heating rate exhibit T_p values of 804-847°C. It is observed that the crystallization peaks of MnO-doped zinc borosilicate glass of Mn:Zn ratios 0.005, 0.01, and 0.015 are relatively unaffected by the MnO content when heated at a 20°C/min heating rate, however, the existence of MnO in the composition reduced crystallization and melt peak height in comparison to zinc borosilicate glass, which contained no MnO. When heated at a 10°C/min heating rate the compositions of Mn:Zn ratios 0 and 0.015 form crystallization peaks that are reminiscent of the 0 Mn:Zn ratio peak when heated at a 20°C/min heating rate. Conversely, the compositions of Mn:Zn ratios 0.005 and 0.01 form an extremely broadened set of crystallization peaks, indicating a temperature range of overlapping nucleation, growth, and decomposition. The onset melting temperature (T_m) of the materials can be observed in the strong endothermic peak that occurs at higher temperatures, notably 962°C for zinc borosilicate glass, effectively nonexistent for MnO-doped zinc borosilicate glass of Mn:Zn ratios 0.005, 0.01, and 0.015 at a 20°C/min heating rate, and from 951-955°C for all compositions at a 10°C/min heating rate.

It was decided that the T_{ct} value of 875°C in the 20°C/min heat rate samples and the T_m of 10°C/min heat rate samples, 951-955°C, were of interest as temperatures of a crystalline transition nature within the samples and warranted further investigation. Heat-treating samples of all four compositions at those temperatures followed by rapid cooling would be used to study the crystalline phases formed in these glasses.

B. Phase Composition

Samples of MnO-doped zinc borosilicate glass of Mn:Zn ratios 0, 0.005, 0.01, and 0.015 heat-treated at the T_{ct} 875°C, exhibited relatively sharp peaks in XRD data that were determined to closely match zinc borate: $Zn_4O(BO_2)_6$ (PDF 01-076-0917), willemite: Zn_2SiO_4 (PDF 04-008-0329), and manganese zinc silicate: $(ZnMn)SiO_4$ (PDF 01-080-2739), with some peak shift of , as seen in Figures 4 and 5. XRD analysis of a sample that had undergone heat-treatment to ≈ 954°C at a rate of 10°C/min, and was subsequently mixed with high purity Si standard, was utilized to determine what amount of observed peak shift could be attributed to instrument error. As seen in Figure 3, ≈ -0.07°2Θ peak shift can be attributed to differences in the equipment utilized to measure the PDF data and our data. This only accounts for half of the measured peak shift.

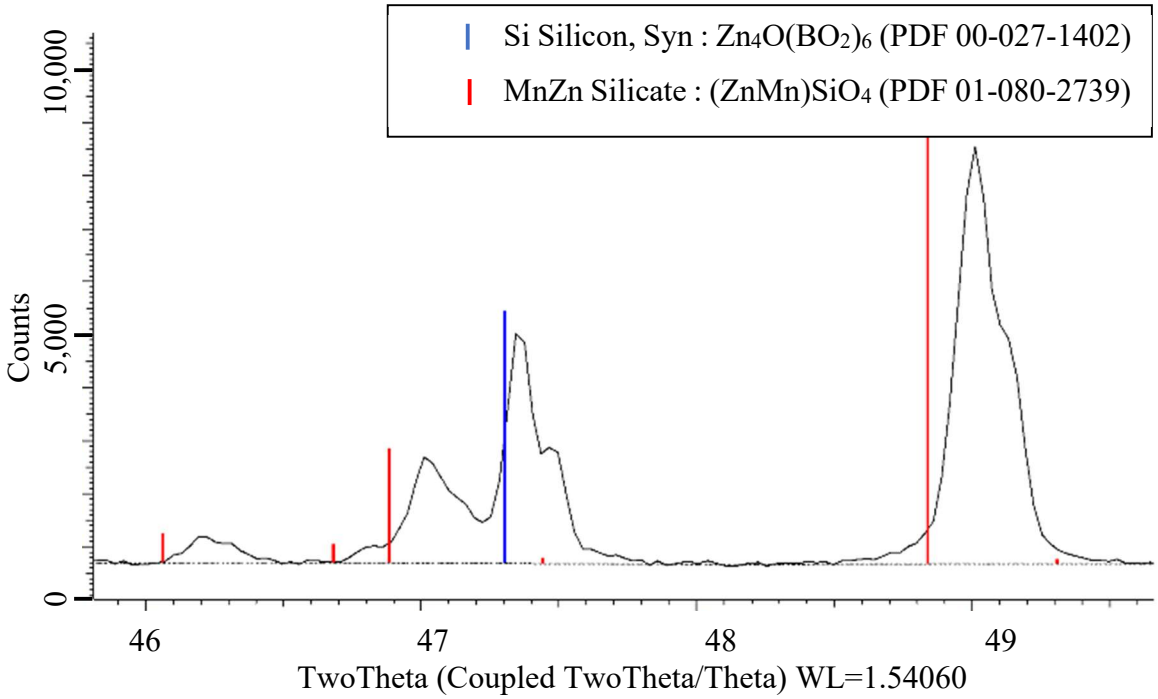

Figure 3: XRD Peaks of MnO-doped zinc borosilicate glass powder heat-treated at 951°C via 10°C/min ramp and mixed with high purity Si standard material to account for instrument error in peak shift.

Samples heat-treated to ≈ 954°C at a rate of 10°C/min exhibited no peaks for zinc borate in comparison to heat-treatment to 875°C at a rate of ≈ 20°C/min as seen in Figures 4 and 5(b). Zinc borate and manganese zinc silicate peaks were observed with a slight peak near 49°2Θ indicating willemite content, as shown in Figure 5(a). Comparatively, no peaks

indicating manganese borate crystallites were observed. XRD peaks of samples treated at the T_m with a 10°C/min heating rate, heat-treatment to ≈ 954°C exhibited a predicted peak shift away from willemite PDF 2Θ values and towards manganese zinc silicate PDF 2Θ values, showing a positive correlation between MnO content and manganese zinc silicate formation.

A sample of MnO-doped zinc borosilicate glass of Mn:Zn ratio 0.005 was separated into two separate particle sizes of greater and less than 250 μm in order to determine whether there was any noticeable change in zinc borate that might indicate an increase or decrease in oxygen content, as the zinc borate phase has the largest atomic% of expected phases, and adsorption due to changes in total sample surface area. The sample of particle size < 250 μm, which had a greater surface area to volume ratio, exhibited with greater intensity, in comparison to other peaks of the same XRD measurement, all peaks other than the peak at 51.7°2Θ, as seen in Figure 6. This peak represents the only zinc borate peak in the spectra for which the peak intensity of the particle size > 250 μm, which had lesser surface area to volume ratio, is greater. Other than this peak, zinc borate and manganese zinc silicate exhibit little change in relation to particle size, indicating that the sample experiences little to no additional oxidation effects dependent on surface area to volume ratio.

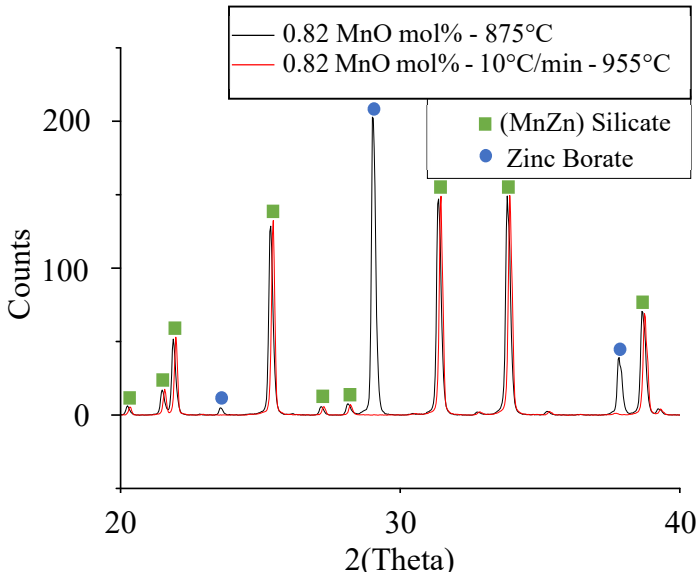

Figure 4: XRD peaks of MnO-doped zinc borosilicate glass powder, of Mn:Zn ratio 0.015:1 (0.82 MnO mol%), post heat-treatment to 875°C at 20°C/min and 951°C at 10°C/min.

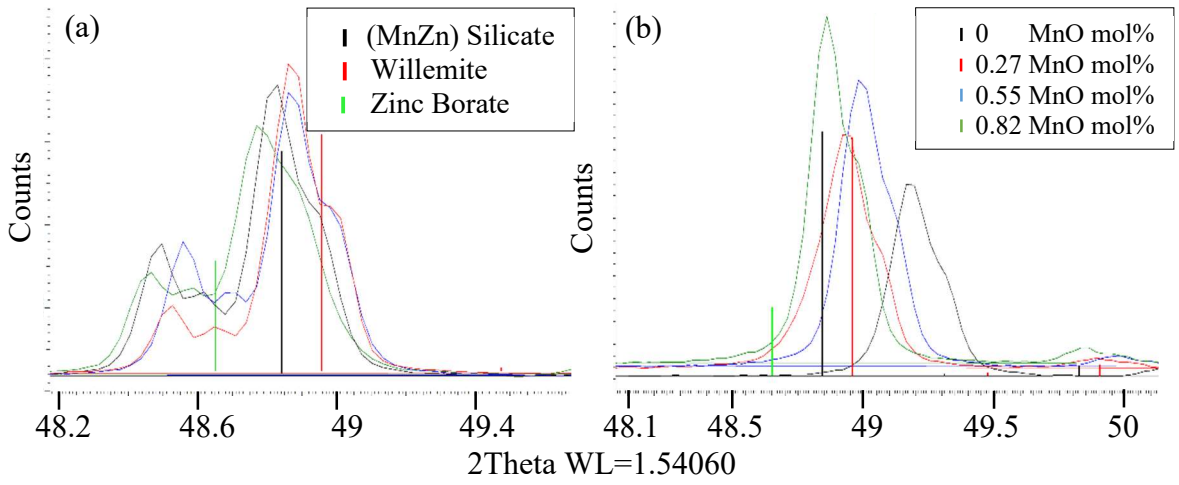

Figure 5: XRD peaks of MnO-doped zinc borosilicate glass powder, (a) after heat-treating at 875°C and (b) after heat-treating at approximately 955°C with a 10°C/min heat rate, where the Mn:Zn ratios are 0, 0.005, 0.01, and 0.015 for compositions of MnO mol% 0 – 0.82 respectively.

It has been found that having a high $ZnO:B_2O_3$ ratio, such as the ≈ 55:20 mol% ratio used in this thesis, can support the formation of greater volumes of willemite and lesser zinc borate.[4] The XRD peaks indicate otherwise with relatively similar peak intensity depending on peak location. This most likely is due to the fact the full crystallization at T_p has not occurred. Instead, partial crystallizations have been induced by heat-treatment at a T_{ct} and at the T_m of the material.

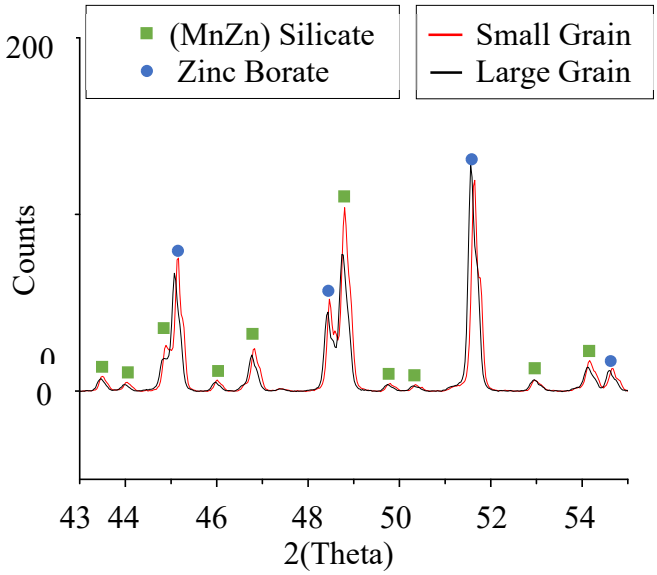

Figure 6: Mn-doped zinc borosilicate glass powder XRD peaks for particle size, of greater and less than 250 µm, comparison.

Rietveld Structural Refinement

Rietveld structural refinement was used to determine the approximate percentage of willemite, manganese zinc silicate, and zinc borate present in the tested samples, as reported in Tables II-V from analysis of Figures 7-14. The (MnO,ZnO)B_2O_3-SiO glass powder that underwent heat-treatment at 20°C/min to 875°C, the transitional point between two crystal maxima, show no significant increase or decrease in willemite, manganese zinc silicate, and zinc borate in relation to the Mn:Zn ratio post heat-treatment, maintaining approximately 35.7% zinc borate. The only exception being the MnO-doped zinc borosilicate glass powder of Mn/Zn ratio 0.005:1, which exhibited the lower 23.7% zinc borate content. It is interesting to note that the amount of crystalline zinc borate detected within the samples, in ratio to the willemite/manganese zinc silicate content, suggests that the detected zinc borate does not account for all of the B_2O_3 present in the sample due to the formation of a glass phase containing B_2O_3 as the initial mol% ratio of B_2O_3 to SiO_2 utilized in sample preparation was approximately 20:25. The chemical phase stability observed in this glass-ceramic with a thermal history of rapid temperature fluctuation and heat-treatment at a transition point between crystal maxima is consistent despite the variation in Mn:Zn ratio that was applied. Heat-treatment to 875°C at a heat rate of ≈ 20°C/min samples exhibited a parabolic increase and decrease of both zinc borate and willemite/MnZn silicate crystallite size (Lorentzian) as MnO is added in increasing quantities. As no other factors decidedly correlate with the alterations to crystallite size, it is unclear if an additional factor such as the amount of glass phase formed, temperature/humidity of the room, or powder grinding technique had any effect on the crystallite size.

Samples that underwent heat-treatment to ≈ 954°C at a rate of 10°C/min, heat-treatment to T_m at 10°C/min and holding temperature, indicated extremely low zinc borate content when the sample has a Mn:Zn ratio less than 0.01. Glass compositions with a Mn:Zn ratio of 0.01 or greater exhibited greatly increased zinc borate percentage post heat-treatment to ≈ 954°C at a rate of 10°C/min, ≈ 40-60% zinc borate. Samples containing low Mn content may have had a slightly different coefficient of thermal expansion. This would lead to a different rate of nucleation and crystal growth when cooling from the T_m and

therefore explain the lack of zinc borate crystallites, however no consistent pattern could be discerned from the lattice parameters that support this hypothesis. Alternatively, though there is not enough evidence to be conclusive, the difference could result from greater replacement of manganese into zinc locations in the matrix, allowing for the creation of more zinc borate. The crystal size Lorentzian of the zinc borate phase post heat-treatment to ≈ 954°C at a rate of 10°C/min was measured to be between 0.5-4.2 nm in glass compositions containing MnO, a notable difference from the ≈ 150-250 nm exhibited by the same compositions following heat-treatment to 875°C at ≈ 20°C/min. The difference suggests smaller crystallites in a more predominant glass phase formed via cooling a sample at the T_m rather than at the T_{ct}, which would contain more fully developed crystallites. The crystal size Lorentzian measured for the ≈ 954°C heat-treatment is so small that it calls into question whether crystallites are even forming in the T_m based heat-treatment, or whether the detected "crystallites" are instead protocrystals.

Table II: Rietveld structural refinement for post heat-treatment zinc borosilicate glass powder XRD peaks. Analyzed in comparison to $Zn_4O(BO_2)_6$ (PDF 01-076-0917) and willemite: Zn_2SiO_4 (PDF 04-008-0329) phases.

		Phase 1	**Phase 2**	**Phase 1**	**Phase 2**
		(Inserted at Temp. held at 875°C)		**(Rate: 10°C/min, held at 955°C)**	
Predicted Phase Content		Zinc Borate	Willemite	Zinc Borate	Willemite
Quantitative Analysis - Rietveld		35.559 %	64.441 %	0.070 %	99.930 %
Space Group		I-43m	R-3	I-43m	R-3
Bragg R Value		4.039	14.444	13.305	16.996
Cry. size Lorentzian (nm)		232.0	183.1	9997.7	123.2
Crystal Linear Absorption Coefficient (1/cm)		140.609	193.639	178.627	193.880
Crystal Density (g/cm^3)		4.238	4.262	5.384	4.267
Lattice Parameters	a (Å)	7.4814(13)	13.9311(46)	6.9077(93)	13.9239(7)
	c (Å)		9.2990(1)		9.2970(5)

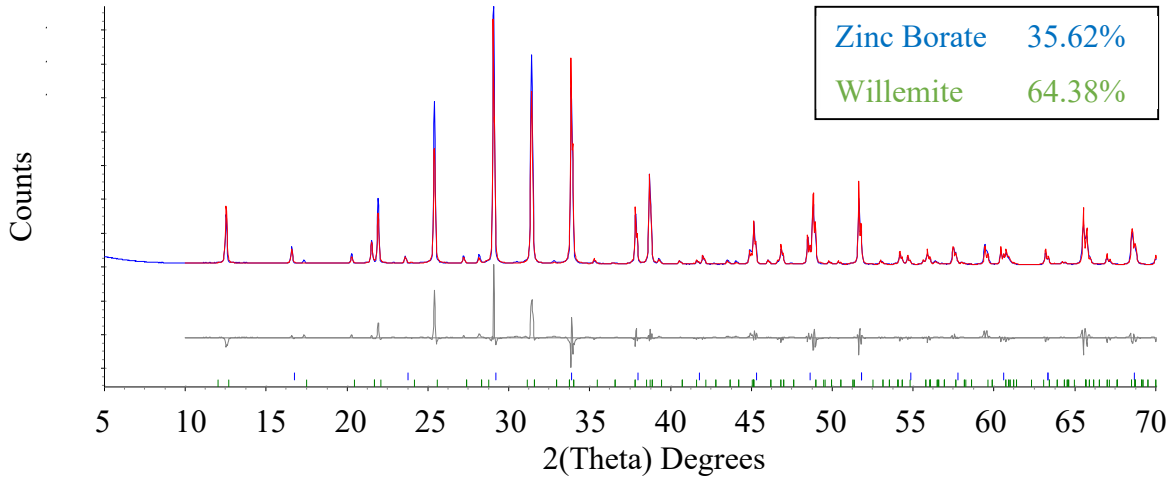

Figure 7: Rietveld structural refinement for post heat-treatment, held at 875°C, zinc borosilicate glass powder XRD peaks. Analyzed in comparison to $Zn_4O(BO_2)_6$ (PDF 01-076-0917) and willemite: Zn_2SiO_4 (PDF 04-008-0329) phases.

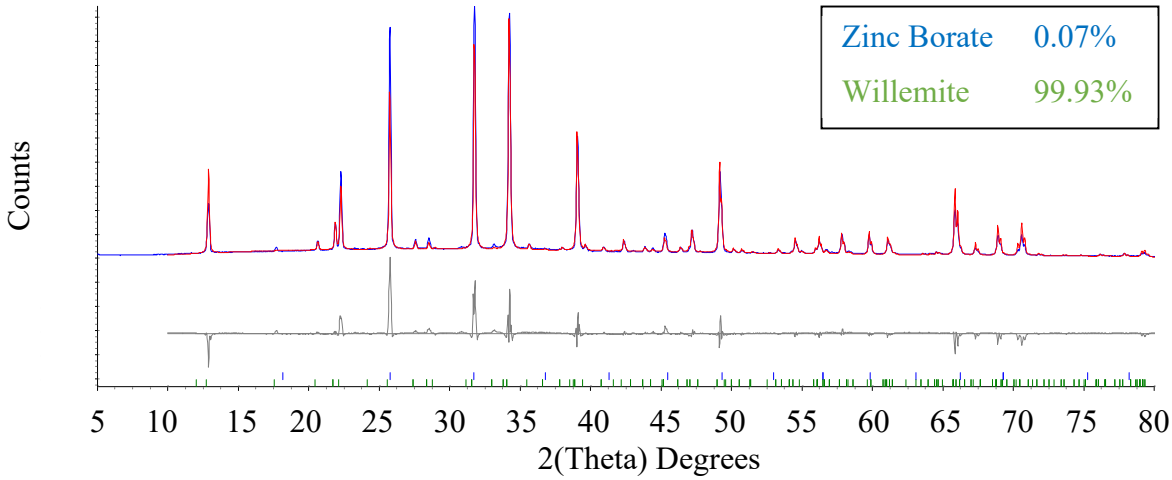

Figure 8: Rietveld structural refinement for post heat-treatment, ramped to and held at 955°C at a rate of 10°C/min, zinc borosilicate glass powder XRD peaks. Analyzed in comparison to $Zn_4O(BO_2)_6$ (PDF 01-076-0917) and willemite: Zn_2SiO_4 (PDF 04-008-0329) phases.

Table III: Rietveld structural refinement for post heat-treatment MnO-doped zinc borosilicate glass powder, of Mn/Zn ratio 0.005:1, XRD peaks. Analyzed in comparison to $Zn_4O(BO_2)_6$ (PDF 01-076-0917), and manganese zinc silicate: $(ZnMn)SiO_4$ (PDF 01-080-2739) phases.

		Phase 1	**Phase 2**	**Phase 1**	**Phase 2**
		(Inserted at Temp. held at 875°C)		**(Rate: 10°C/min, held at 955°C)**	
Predicted Phase Content		Zinc Borate	Manganese Zinc Silicate	Zinc Borate	Manganese Zinc Silicate
Quantitative Analysis - Rietveld		23.682 %	76.318 %	2.551 %	97.449 %
Space Group		I-43m	R-3	I-43m	R-3
Bragg R Value		7.774	6.614	2.845	3.115
Cry. size Lorentzian (nm)		269.2	209.9	4.2	98.2
Crystal Linear Absorption Coefficient (1/cm)		140.666	201.826	137.168	201.327
Crystal Density (g/cm^3)		4.240	4.262	4.135	4.251
Lattice Parameters	a (Å)	7.4804	13.9305(5)	7.5434(55)	13.9356(82)
	c (Å)		9.2899(61)		9.3061(48)

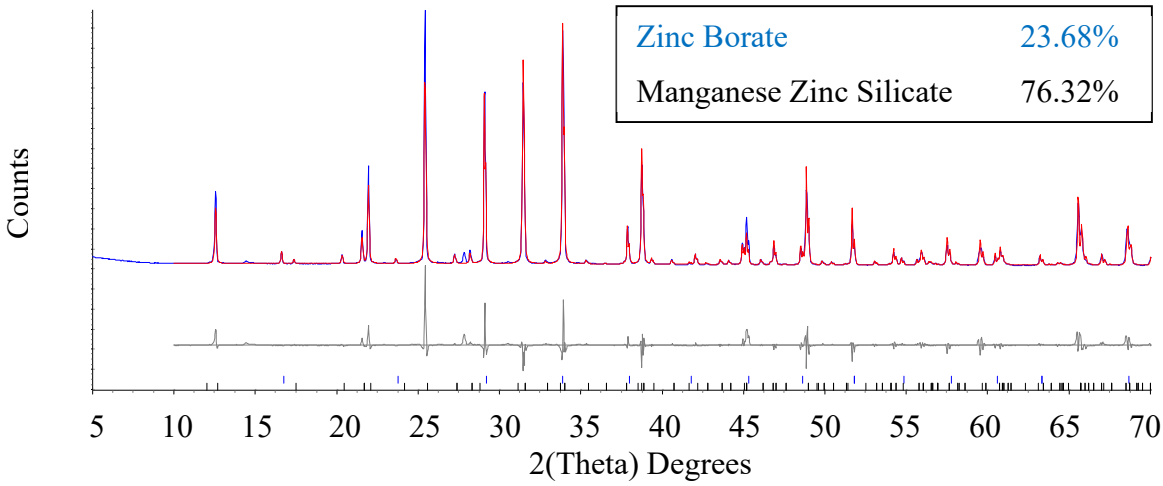

Figure 9: Rietveld structural refinement for post heat-treatment, held at 875°C, MnO-doped zinc borosilicate glass powder, of Mn:Zn ratio 0.005:1, XRD peaks. Analyzed in comparison to $Zn_4O(BO_2)_6$ (PDF 01-076-0917) and willemite: Zn_2SiO_4 (PDF 04-008-0329) phases.

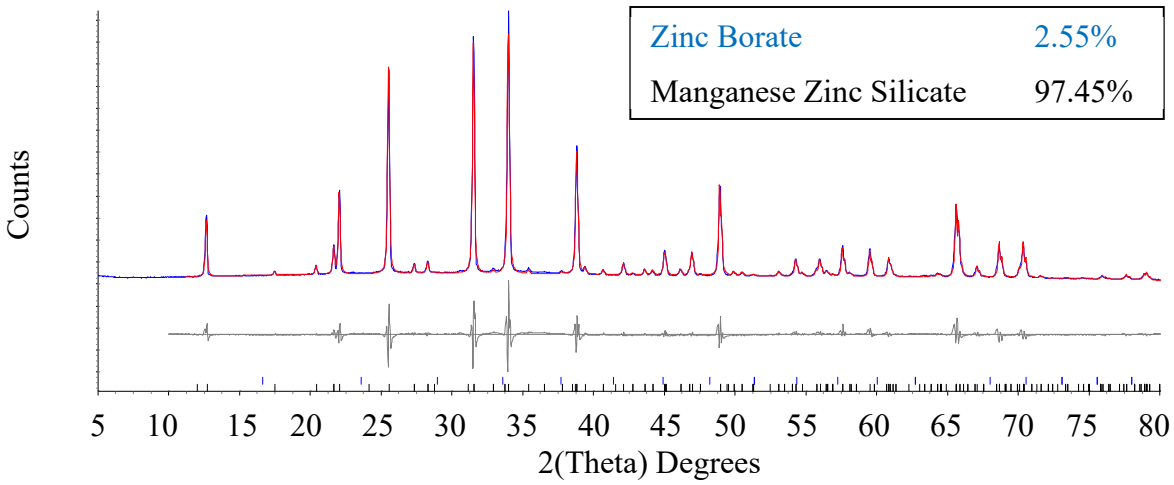

Figure 10: Rietveld structural refinement for post heat-treatment, ramped to and held at 955°C at a rate of 10°C/min, MnO-doped zinc borosilicate glass powder, of Mn:Zn ratio 0.005:1, XRD peaks. Analyzed in comparison to $Zn_4O(BO_2)_6$ (PDF 01-076-0917) and willemite: Zn_2SiO_4 (PDF 04-008-0329) phases.

Table IV: Rietveld structural refinement for post heat-treatment MnO-doped zinc borosilicate glass powder, of Mn/Zn ratio 0.01:1, XRD peaks. Analyzed in comparison to $Zn_4O(BO_2)_6$ (PDF 01-076-0917), and manganese zinc silicate: $(ZnMn)SiO_4$ (PDF 01-080-2739) phases.

		Phase 1	**Phase 2**	**Phase 1**	**Phase 2**
		(Inserted at Temp. held at 875°C)		**(Rate: 10°C/min, held at 955°C)**	
Predicted Phase Content		Zinc Borate	Manganese Zinc Silicate	Zinc Borate	Manganese Zinc Silicate
Quantitative Analysis - Rietveld		36.634 %	63.366 %	63.206 %	36.794 %
Space Group		I-43m	R-3	I-43m	R-3
Bragg R Value		3.624	4.927	1.594	3.460
Cry. size Lorentzian (nm)		241.3	190.6	0.5	141.0
Crystal Linear Absorption Coefficient (1/cm)		140.733	201.530	193.308	201.419
Crystal Density (g/cm^3)		4.242	4.255	5.827	4.253
Lattice Parameters	a (Å)	7.4792(11)	13.9313(68)	6.7282(97)	13.9340(18)
	c (Å)		9.3024(95)		9.3040(79)

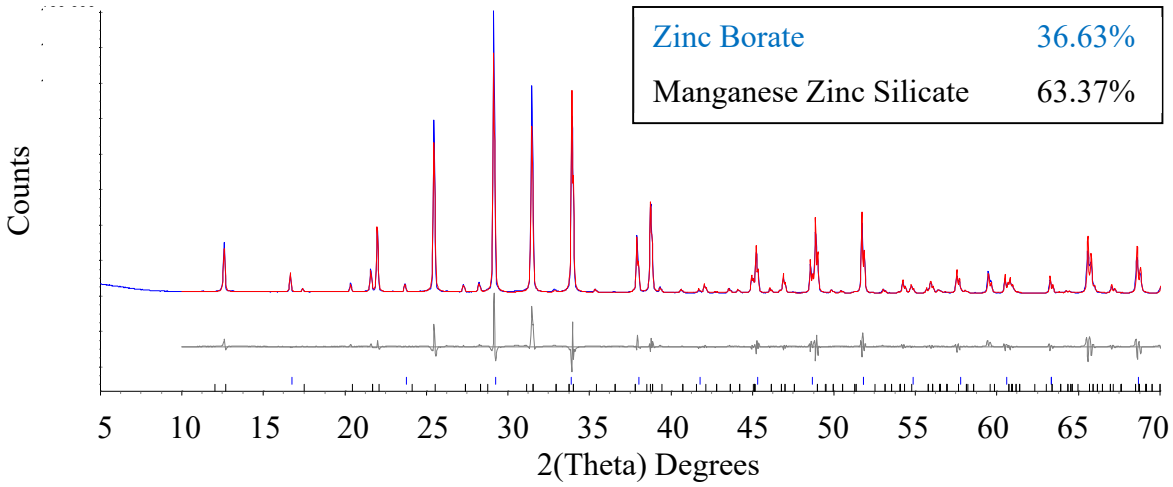

Figure 11: Rietveld structural refinement for post heat-treatment, held at 875°C, MnO-doped zinc borosilicate glass powder, of Mn:Zn ratio 0.01:1, XRD peaks. Analyzed in comparison to $Zn_4O(BO_2)_6$ (PDF 01-076-0917) and willemite: Zn_2SiO_4 (PDF 04-008-0329) phases.

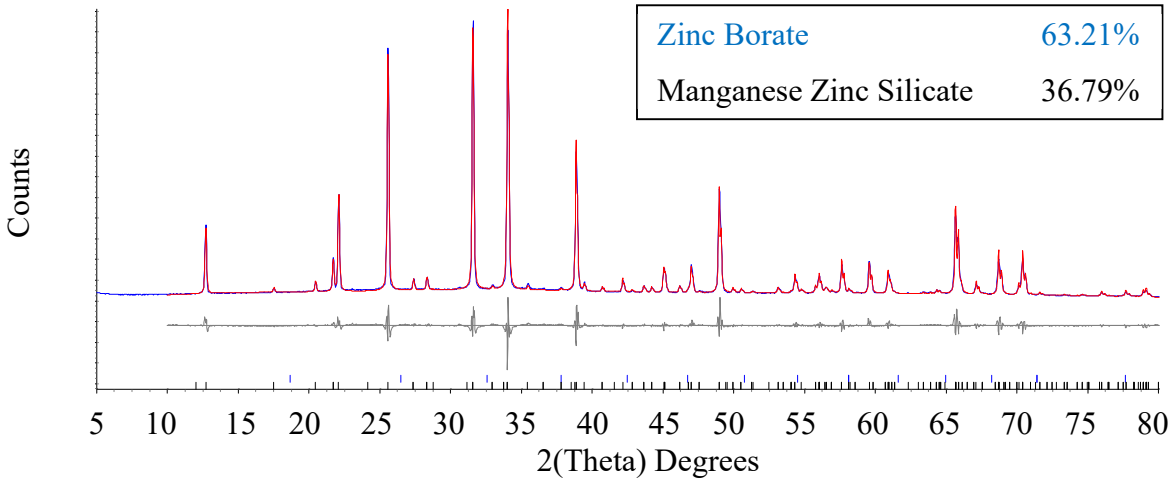

Figure 12: Rietveld structural refinement for post heat-treatment, ramped to and held at 955°C at a rate of 10°C/min, MnO-doped zinc borosilicate glass powder, of Mn:Zn ratio 0.01:1, XRD peaks. Analyzed in comparison to $Zn_4O(BO_2)_6$ (PDF 01-076-0917) and willemite: Zn_2SiO_4 (PDF 04-008-0329) phases.

Table V: Rietveld structural refinement for post heat-treatment MnO-doped zinc borosilicate glass powder, of Mn/Zn ratio 0.015:1, XRD peaks. Analyzed in comparison to $Zn_4O(BO_2)_6$ (PDF 01-076-0917), and manganese zinc silicate: $(ZnMn)SiO_4$ (PDF 01-080-2739) phases.

		Phase 1	**Phase 2**	**Phase 1**	**Phase 2**
		(Inserted at Temp. held at 875°C)		**(Rate: 10°C/min, held at 955°C)**	
Predicted Phase Content		Zinc Borate	Manganese Zinc Silicate	Zinc Borate	Manganese Zinc Silicate
Quantitative Analysis - Rietveld		34.849 %	65.151 %	38.735 %	61.265 %
Space Group		I-43m	R-3	I-43m	R-3
Bragg R Value		3.518	2.694	0.327	1.830
Cry. size Lorentzian (nm)		145.8	112.9	0.6	165.2
Crystal Linear Absorption Coefficient (1/cm)		140.512	201.282	192.924	201.302
Crystal Density (g/cm^3)		4.236	4.250	5.815	4.251
Lattice Parameters	a (Å)	7.4831(45)	13.9371(39)	6.7327(57)	13.9365(45)
	c (Å)		9.3062(57)		9.3061(21)

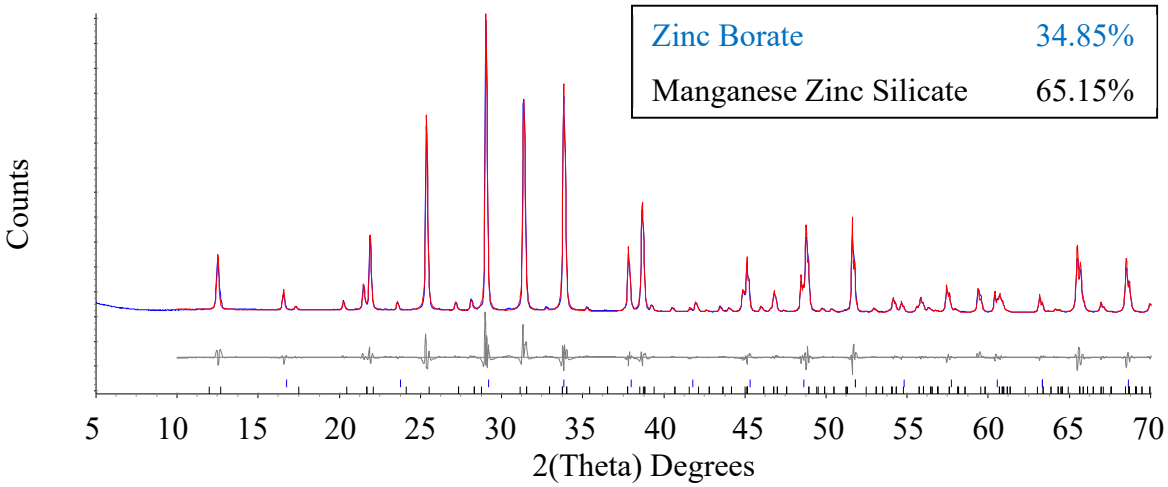

Figure 13: Rietveld structural refinement for post heat-treatment, held at 875°C, MnO-doped zinc borosilicate glass powder, of Mn:Zn ratio 0.015:1, XRD peaks. Analyzed in comparison to $Zn_4O(BO_2)_6$ (PDF 01-076-0917) and willemite: Zn_2SiO_4 (PDF 04-008-0329) phases.

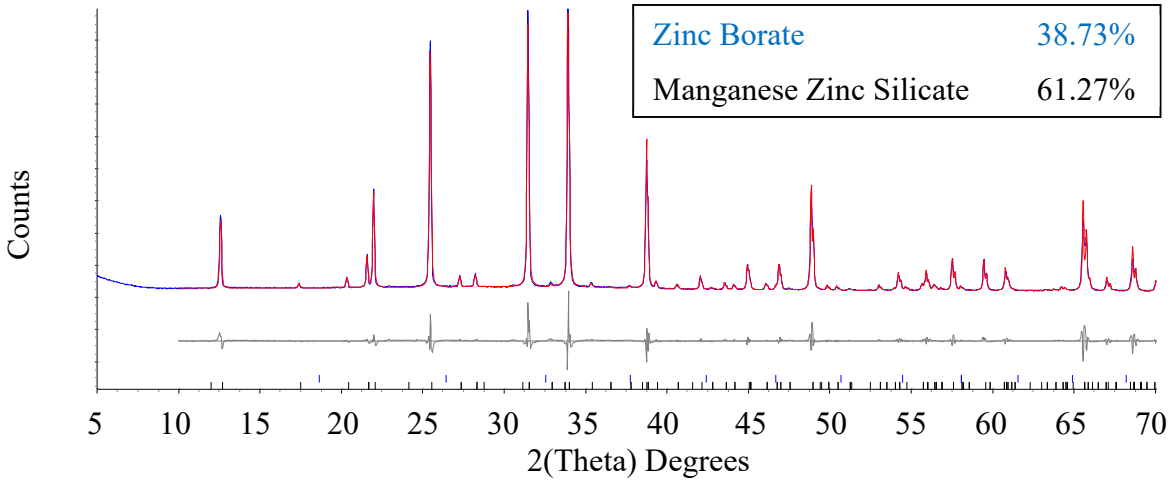

Figure 14: Rietveld structural refinement for post heat-treatment, ramped to and held at 955°C at a rate of 10°C/min, MnO-doped zinc borosilicate glass powder, of Mn:Zn ratio 0.015:1, XRD peaks. Analyzed in comparison to $Zn_4O(BO_2)_6$ (PDF 01-076-0917) and willemite: Zn_2SiO_4 (PDF 04-008-0329) phases.

SEM Imaging and EDS Chemical Analysis

SEM spot analysis and EDS chemical mapping, as shown if Figure 15-20, were used to further analyze the surface of sample crystallites for comparison with the expected chemical composition found by XRD and Rietveld structural refinement. The findings of the chemical mapping were in relatively close agreement with the Rietveld data, with exception to the fact that this surface analysis technique was incapable of properly identifying boron content due to the inherent difficulty of the impinging electrons interacting with an element of a low atomic number. In Figure 15, B and Mn contents of zinc borosilicate glass was at 2%, indicating the expected inability to properly detect boron, as the original composition is 20 mol % B_2O_3, and a case of forced false positive, as zinc borosilicate glass contains no manganese. Based on the O and Zn contents, the crystallites observed in Figure 15 are attributed to either a zinc borate formation, which has hexagonal structures, or pure zinc oxide crystallites. The observed formations resemble the reverse crystal growth of ZnO microdisks studied by Self et al.[14] Although willemite is also known to form trigonal and hexagonal crystal systems there was minimal silicon detected at these locations when compared to zinc and oxygen. Minimal silicon, in comparison to zinc and oxygen, was observed throughout the sample. There were also areas that exhibited a mixture of zinc and silica, where the expected zinc silicate would form.

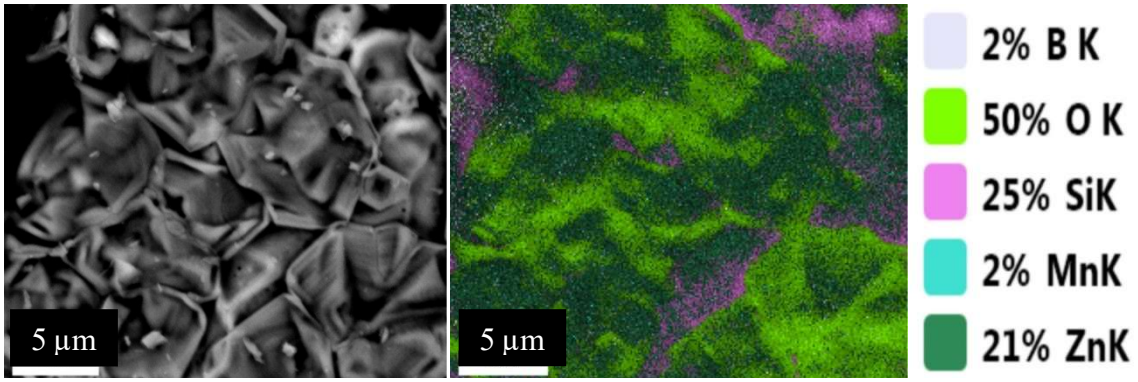

Figure 15: EDS elemental mapping of zinc borosilicate glass powder heat-treated at 875°C, Au-sputter coated, and utilizing back scattering electrons.

Chemical mapping and EDS imaging of MnO-doped zinc borosilicate glass of Mn:Zn ratio 0.005 revealed three structures of interest; the first of which is the lighter colored formations, fractured from the grinding process, which are formations of zinc borate as can be seen by the O and Zn contents in Figure 16. Mn content can only be observed in locations where Zn can be directly observed, as expected due to Mn replacing Zn locations in the matrix. This would suggest the existence of a manganese borate phase, however the lack of XRD peak pattern identifying manganese borate under the same conditions at which zinc borate was formed suggests either a zinc borate or manganese zinc silicate priority over manganese borate.

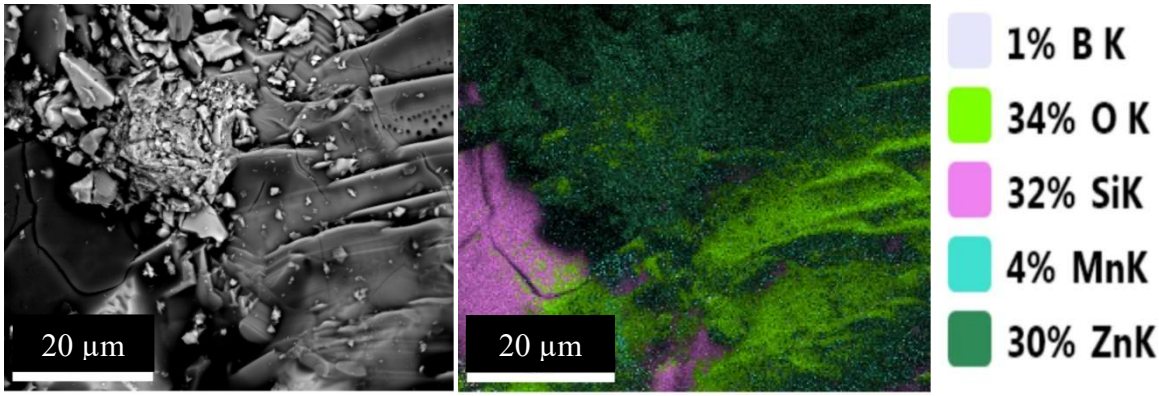

Figure 16: EDS elemental mapping of MnO-doped zinc borosilicate glass powder, of Mn:Zn ratio 0.005:1 for composition of MnO mol% 0.27, heat-treated at 875°C, Au-sputter coated, and utilizing back scattering electrons. Map 1

The second structural feature of interest is the formation of pores that appear in some sections of the zinc borate experiencing additional surface oxidation, seen in Figures 16 and 17. These pores are potentially pockets left over from locations where materials

were oxidized off but were trapped in the melt. While excessive bubbling was not observed in the glass samples during sample preparation, micron scale bubbles may have gone unnoticed.

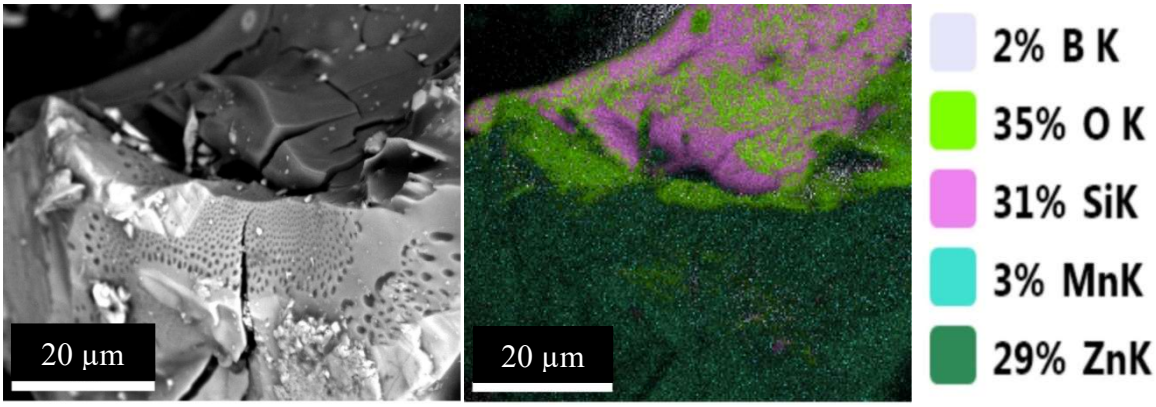

Figure 17: EDS elemental mapping of MnO-doped zinc borosilicate glass powder, of Mn:Zn ratio 0.005:1 for composition of MnO mol% 0.27, heat-treated at 875°C, Au-sputter coated, and utilizing back scattering electrons. Map 2

The third structure appeared to be primarily occupied by silica and exhibits a lack of zinc, therefore it is considered that the phase, seen in Figures 16, 17, and 18, is crystalline or glassy SiO_2 phase. The lack of Zn, Mn, or B presence suggests that this is a glass phase and that the zinc borate and willemite/Mn Zn silicate phases detected via XRD may be the two lighter colored phases observed in Figure 18.

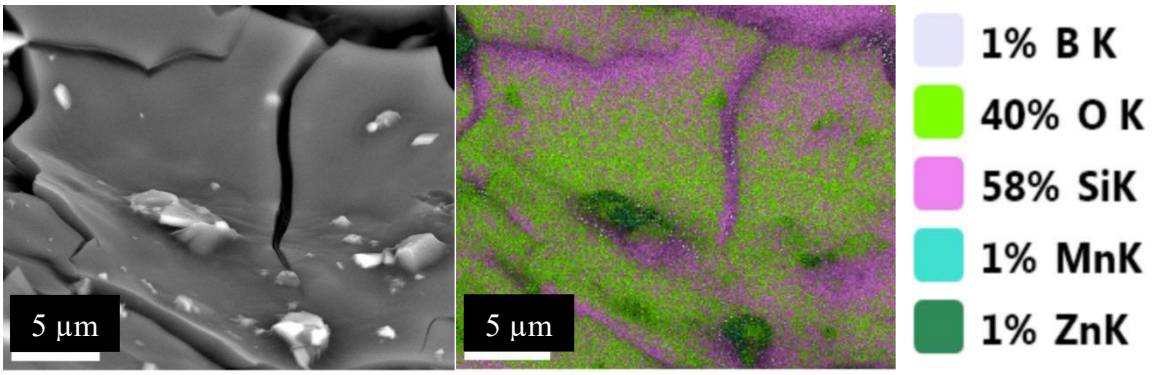

Figure 18: EDS elemental mapping of MnO-doped zinc borosilicate glass powder, of Mn:Zn ratio 0.005:1 for composition of MnO mol% 0.27, heat-treated at 875°C, Au-sputter coated, and utilizing back scattering electrons. Map 3

A sample of MnO-doped zinc borosilicate glass of Mn:Zn ratio 0.015, under heat-treatment to 875°C at ≈ 20°C/min exhibited a structure, formed of primarily Zn that

appeared hexagonal in sections with raised boundaries (like walls) made of a mixture of O and Zn, as seen in Figure 19. Similar to the structures observed in Figure 15, and those studied by Self et al. [14], these formations are understood to be a form of fractured zinc oxide microdisks. The deformation of the hexagonal structure is due to either modification to a zinc borate phase, or the heat-treatment at the transition point between two crystal maxima causing the crystallites to deform. The hexagonal structures formed, most likely via heterogeneous nucleation, above and next to what appear to be either a crystalline willemite, manganese zinc silicate, or glass silicate phase.

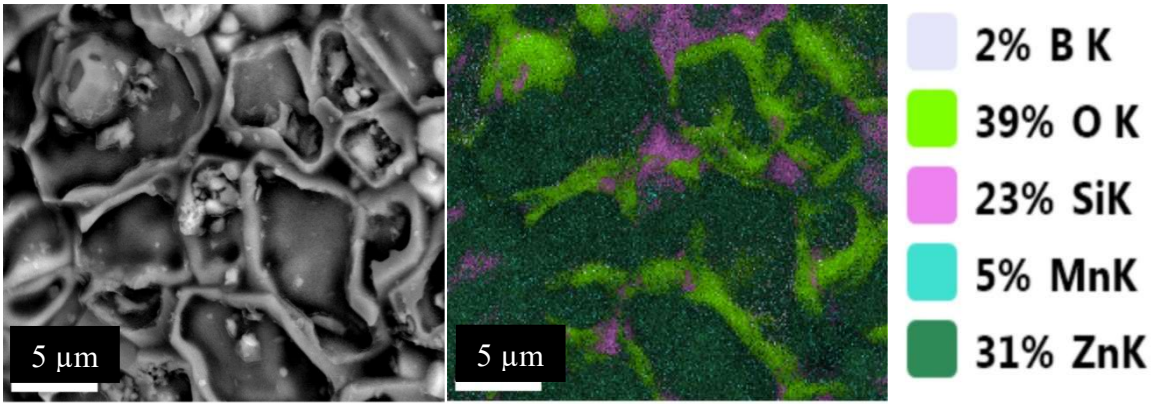

Figure 19: EDS elemental mapping of MnO-doped zinc borosilicate glass powder, of Mn:Zn ratio 0.015:1 for composition of MnO mol% 0.82, heat-treated at 875°C, Au-sputter coated, and utilizing back scattering electrons.

Counter to the varied structures found in samples post heat-treatment to 875°C at a rate of ≈ 20°C/min, heat-treatment to ≈ 954°C at a rate of 10°C/min samples consistently exhibited the three structures seen in Figure 20. The three notable structures consisted of inclusions of SiO_2, observed in yellow (Si), light green (O), and a distinct lack of dark green (Zn) in Figure 20, which had broken from the surrounding phases due to a differing rate of thermal expansion. There exists occasionally a porous phase, pores potentially due to SiO_2 inclusions, mixed intermittently with a smooth phase, both containing comparable Zn content. These phases can be differentiated via O and Si content to be willemite/(Mn,Zn)silicate and zinc borate, respectively. Neither B nor Mn could be detected sufficiently to map in any of the four glass compositions.

.

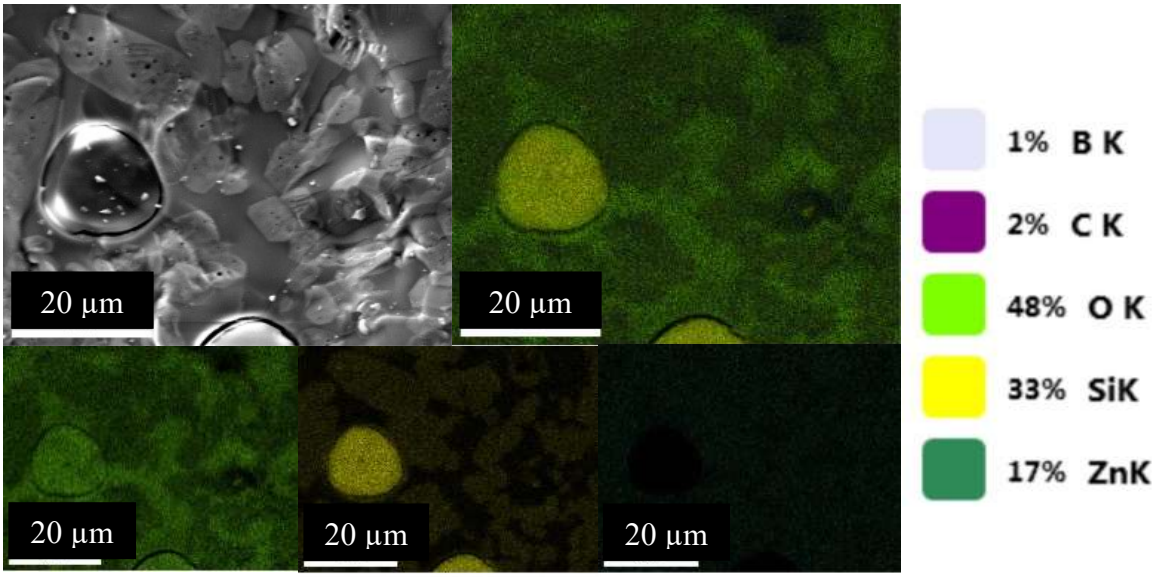

Figure 20: EDS elemental mapping of MnO-doped zinc borosilicate glass powder heat-treated to 955°C at a rate of 10°C/min, Au-sputter coated, and utilizing back scattering electrons.

IV. SUMMARY AND CONCLUSIONS

MnO-doped zinc borosilicate glass of Mn:Zn ratios 0.005:1, 0.01:1, and 0.015:1 heat-treated at a rate of 20°C/min were found to be relatively resistant to induced structural alteration via rapid heating rates, as DSC peaks exhibited were relatively broad and exhibited few rapid changes in heat flow. When heat-treated at the transition point between two crystalline maxima, 875°C, samples exhibited a variety of structures as a glass-ceramics of consistent zinc borate and willemite / (Mn,Zn) silicate crystalline phase percentages, regardless of Mn:Zn ratio and no manganese borate. Samples heat-treated to the T_m, ≈ 955°C, at a rate of 10°C/min showed nucleation of SiO_2 inclusions and willemite / manganese zinc silicate crystallites in a zinc borosilicate glass / protocrystal matrix, with increasing zinc borosilicate with Mn:Zn ratio.

V. FUTURE WORK

Given the opportunity to continue this work, focus would be on slower and faster femtolaser rastering speeds, slower heating rates, and the effects of higher Mn:Zn ratios, as these aspects were either incomplete or could be explored further. There is potential that if the rastering speed is slow enough, the energy applied will be able to consistently cause etching, ablation or crystallization, the effects of which is worth investigating. Although a general trend of the effects of the MnO dopant on select properties at these ratios was established, it would be worthwhile to expand the selection of data points to see how the effects may change. An area of interest that should be fully explored is the source and mechanics controlling the incredibly regular bubble pattern observed in both Figures 16 and 17. Additionally, future work determining the exact nature and source of the nano-wires observed post heat-treatment and laser application would be appropriate.

VI. APPENDIX – ADDITIONAL WORK COMPLETED

A. Sample Preparation

The four polished samples, prior to and post laser irradiation, were used for terahertz time-domain spectroscopy (THz-TDS – TPS Spectra 3000, TeraView, Cambridge, UK) measurements over 0 – 4 THz frequencies to determine changes in optical and dielectric properties induced by femtosecond laser irradiation. Fluorescence spectroscopy (F-7000, Scientific Inc, Massachusetts, USA) of cut and polished samples was utilized to measure emission from 200-900 nm under 337 nm excitation. Additionally, the laser-irradiated sample regions were examined via Raman spectroscopy (Alpha300, WITec focus innovations, Lise-Meitner-Str. 6, D-89081 Ulm, Germany) from wavenumber 0 to 4300, at low energy to avoid sample fluorescence caused by Mn present in the samples, and UV/Vis spectroscopy was used to examine potential color alterations in the semi-transparent glass samples.

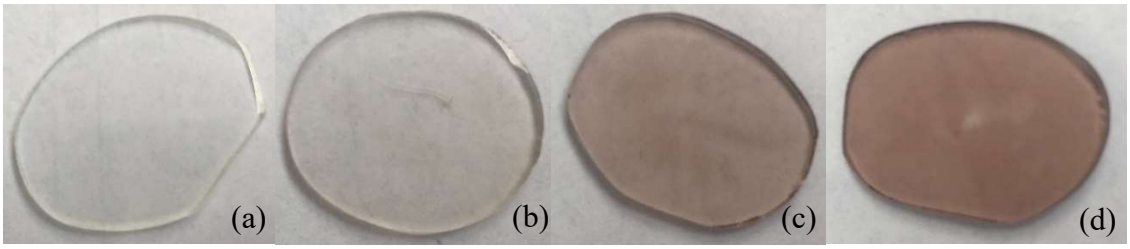

Figure A1: Cut, ground, and polished samples of MnO-doped zinc borosilicate glass, of Mn/Zn ratios 0, 0.005, 0.01, and 0.015 for compositions of MnO mol% 0 – 0.82 respectively(a-d).

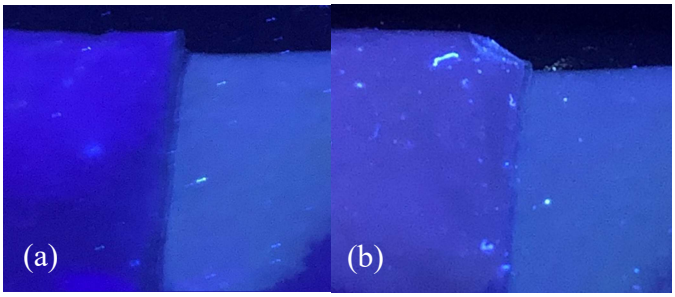

Figure A2: MnO-doped zinc borosilicate glass powder, of Mn/Zn ratios 0:1 and 0.015:1(a) and 0.01:1 and 0.015(b) for compositions of MnO mol% 0.55 and 0.82 respectively under UV light. Post heat-treatment at 10C/min to ≈ 955°C. Exhibiting the 0 photoluminescence, 0:1 Mn:Zn, reddish orange photoluminescence generated via glass containing Mn^{3+}, 0:01:1 Mn:Zn, and the yellow-green produced via ceramic containing Mn^{2+}.

B. Femtosecond Laser Irradiation and Optical Characterization

We have used a Scientific XL 500 Femtolaser (Spectraphysics) to induce nonlinear absorption of laser energy into glass samples with the goal of localized high temperature material alteration within a larger cold body.[10-11] The fs-laser utilizes a mode locking technique, in which pulses from a Ti:Sapphire source reflect between a pair of mirrors to generate an oscillating longitudinal mode, or set of modes, that outputs a pulse within the cavity at a set interval.[12] This technique allows for the generation of laser pulses that, due to the high-energy level and compressed time span of the modified pulse, can induce non-linear adsorption constrained to a localized area by the size of the focused laser's focal point. Non-linear adsorption refers to the situation where, rather than transmitting through a relatively transparent piece of glass, the high intensity of a beam of light causes the atoms of a structure to ionize through multiple energy events that do not give the atoms time to return to their rest state, thereby absorbing the high intensity light. The localized area of effect inherent in short laser pulses allows the non-linear adsorption mechanic; either photoionization or avalanche ionization, which occurs via laser applied electromagnetic field and atomic impact, to modify glass structure at the surface or sub-surface through the rapid absorption and subsequent dispersion of the energy of each pulse. The depth of modification depends on the depth of focus of the laser pulses. The modification of the glass, caused by localized heating within the larger cold body, can affect morphological, chemical, optical, and structural properties, all of which are potentially useful to be able to directly modify, e.g., change color centers, crystallinity, and refractive index.[10-12]

Solid glass samples were cut and polished to an approximate 3200 grit, on a Metaserv 250 Grinder-Polisher (Buehler), on both sides with a sample thickness of < 2 mm. Femtosecond laser irradiation was completed using a 800 nm laser with a Ti:Sapphire source Scientific XL 500 Femtolaser (Spectra-Physics, Santa Clara, CA, USA). The four samples were exposed to 300 repetitions of laser pulses at two rastering speeds of 1 mm/s and 0.5 mm/s over two 3 mm^2 areas on each sample. The laser power was consistent at approximately 1.75 W, as measured directly prior to irradiation from a point approximately one foot in front of the sample aperture, with only minor drift of ±0.05 W over the course of irradiation.

Femtosecond laser treated locations and untreated locations, shown in Figure A3 below, of samples of MnO-doped zinc borosilicate glass of Mn/Zn ratios 0:1, 0.005:1, 0.01:1, and 0.015:1 exhibit no crystallization or other alteration visible to the naked eye. These results are consistent with the previously found resistance to crystallization exhibited by MnO-doped zinc borosilicate glass of Mn/Zn ratios 0.005:1, 0.01:1, and 0.015:1, specifically those with low MnO content, when heated at a relatively rapid rate. When irradiated with UV light, the samples containing Mn exhibit the expected reddish-orange photoluminescence, due to Mn being included into a non-cubic structure within the zinc borosilicate glass and therefore having a valence greater than 2.[16] The coloration deepens with the increase in manganese content, most likely due to interference from the decreased optical clarity produced by the existence of Mn^{3+} as a colorant in the glass sample.[9]

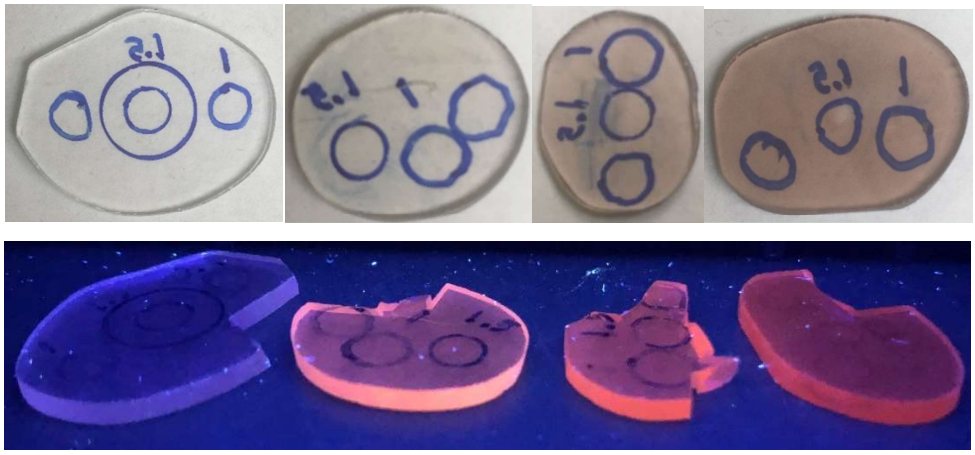

Figure A3: Cut and polished MnO-doped zinc borosilicate glass, of Mn/Zn ratios 0, 0.005, 0.01, and 0.015 for compositions of MnO mol% 0 – 0.82 respectively, pre and post laser application, 1.5 = 1 mm/s and 1 = 0.5 mm/s rastering speed for laser application. Shown in both natural light and UV light.

Heat-treated powder samples that were brought to the T_m value for their respective composition only exhibited the yellow/green coloration expected of a glass-ceramic MnO-ZnO-B_2O_3-SiO_2 system, irradiated with UV light, in MnO-doped zinc borosilicate glass powder of Mn/Zn ratio 0.015:1, the composition with the highest Mn content, as seen in Figure A4.[2,6,9] The green luminescence is caused by Mn^{2+} as part of a cubic structure, while the yellow luminescence is caused by Zn existing in both a glass phase and non-cubic crystalline structures within the material.[16]

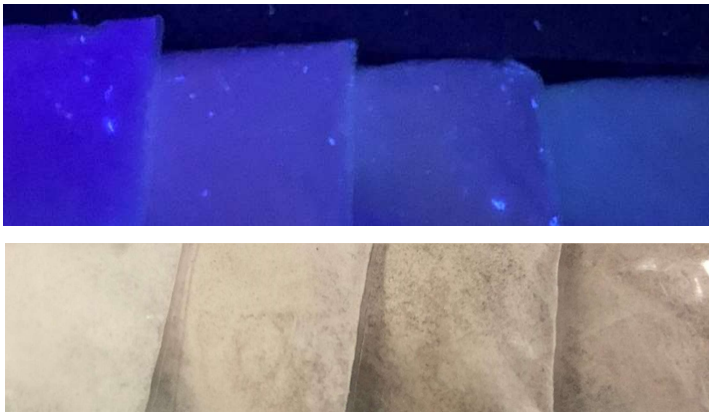

Figure A4: MnO-doped zinc borosilicate glass powder, of Mn/Zn ratios 0, 0.005, 0.01, and 0.015 for compositions of MnO mol% 0 – 0.82 respectively, after heat-treating at 10°C/min to 952,953,954, 955°C respectively.

Heat-treated zinc borosilicate glass powder, of high zinc content, exhibited no photoluminescence, as expected. MnO-doped zinc borosilicate glass powder of Mn/Zn ratio 0.005:1 exhibited photoluminescence similar to the red-orange coloration expected of purely glass samples, while MnO-doped zinc borosilicate glass powder of Mn/Zn ratio 0.01:1 produced red coloration that was tinged with the green/yellow coloration of the glass-ceramic phase. This suggests the shift from a pure glass, with Mn^{3+} and Zn in non-cubic structures, to a glass-ceramic, with Mn^{2+} in a cubic structure and Zn existing in both the remaining glass phase and non-cubic crystalline structures as the manganese content increases.[9,16]

Fluorescence spectroscopy was used to quantify the findings of the visual analysis of sample fluorescence under UV light. A usable excitation wavelength of 337 nm was found from the work of Ehrt et al. on a similar composition of MnO-doped zinc borosilicate.[6] As expected, zinc borosilicate without Mn-doping did not exhibit any fluorescence and MnO-doped zinc borosilicate glass of Mn/Zn ratios 0.005:1, 0.01:1, and 0.015:1exhibited broad peaks that span over ≈ 550-700 nm, as seen in Figure A5, which broaden and increase in intensity as MnO content increases. Those peaks were expected due to visual observation that the emission appeared to be an orange-red coloration, matching the wavelength range found. The dramatic peaks at 337 nm and 677 nm can be ignored as artifacts caused by the excitation frequency and the instrument's radiation source, respectively. It is possible that the peak shift to the right that can be observed as

MnO content increases is not due to the increase in manganese, but is also the peak being affected by the artifact at 677 nm.

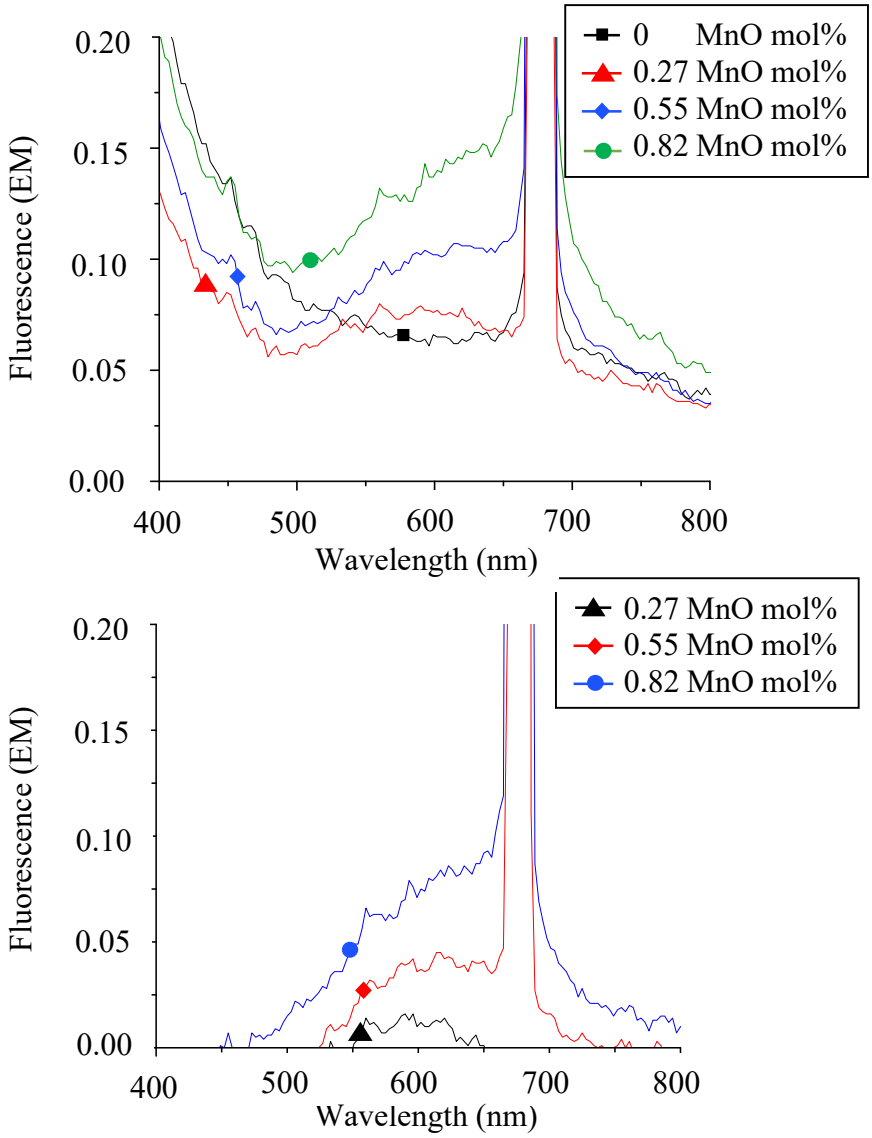

Figure A5: Fluorescence Spectroscopy peaks of MnO-doped zinc borosilicate glass powder, of Mn/Zn ratios 0, 0.005, 0.01, and 0.015 for compositions of MnO mol% 0 – 0.82 respectively(top) and of Mn/Zn ratios 0.005, 0.01, and 0.015, for compositions of MnO mol% 0.27 – 0.82, utilizing Mn/Zn ratios 0:1 as background noise(bottom).

Post-laser irradiation, the polished glass samples were also inspected via SEM imaging, utilizing back-scattering electrons to avoid charging caused by sample photoluminescence, to detect whether laser irradiation at these rastering speeds, and relatively consistent beam energy, had any discernable physical effects on the samples that

were not readily visible to the naked eye. There were few alterations of note, as the glass samples were generally unchanged, however one formation that appeared across most samples, especially those of the slower rastering speed of 0.5 mm/s was a consistent patterning of parallel lines that only occurred at the edges of the treated areas of the samples, where the laser irradiation region overlapped with the Sharpie marker used to mark the treated areas for the naked eye seen below in Figures A6-A7. This low penetration patterning, appearing of less depth than the residual polishing lines visible, appeared to have no correlation to the Mn:Zn ratio of the glass as it appeared in some form on all samples. The disregard of the sample composition, low depth, and lack of appearance on non-Sharpie sections of the samples indicates that this is a thin film scribing that is occurring as the femtolaser burns through the Sharpie marking the samples.

In most locations observed, the samples exhibited only thin film scribing when the Sharpie mark crossed with the treatment area, though the scribing was not continuously present. A couple of the observed locations on samples which had been treated via the slower rastering speed of 0.5 mm/s, exhibit that the fluence of the laser was high enough to exceed the ablation threshold of the glass and briefly produced laser-induced periodic surface structures (LIPSS). These LIPSS appear as ripples near perpendicular to the path of the laser as seen in Figures A6 and A7. This ripple structure occurs during femtosecond laser irradiation when "surface waves in the melt develop as the incoming light interferes with the scattered light off of the material"[17] It should be noted that the LIPSS ripple structures observed were of similar length, ≈ 800 nm, to the wavelength of the femtosecond laser used for irradiation. The varied LIPSS depth is due to some of the ripples self-focusing the femtosecond laser pulses into their valleys, creating a more directed ablation process.[17] It was interesting to note that the LIPSS of MnO-doped zinc borosilicate glass, of Mn/Zn ratio 0.015:1, tends towards consistent parallel formations while those observed in pure, high zinc content, zinc borosilicate glass studied in this thesis exhibit a more varied width and angle. The exact causes of these different effects is not yet understood.

A structure that may be related to the LIPSS can be observed in Figures A7 and A8 as a series of holes that have been punched into the surface of the glass. These holes appear to follow surface defects such as polishing marks and resemble the marking of ns-laser based ablation rather than fs-laser ablation. Notably there are small particles of debris near

the holes, the holes appear rugged rather than smooth cut, and the surface area around the holes is slightly pulled back and damaged, suggesting the impact of extended laser pulse exposure.[17] One possible reason for this formation would be an imperfection in the run-cycle of the fs-laser used in testing, however this would not account for the holes following the irregular surface lines of the samples. Alternatively, this could be caused by the ridges of the imperfections of the glass surface guiding the laser pulses, similarly to how the LIPSS for deeper ripples to alter the surface of the sample, through focused and prolonged energy irradiation.

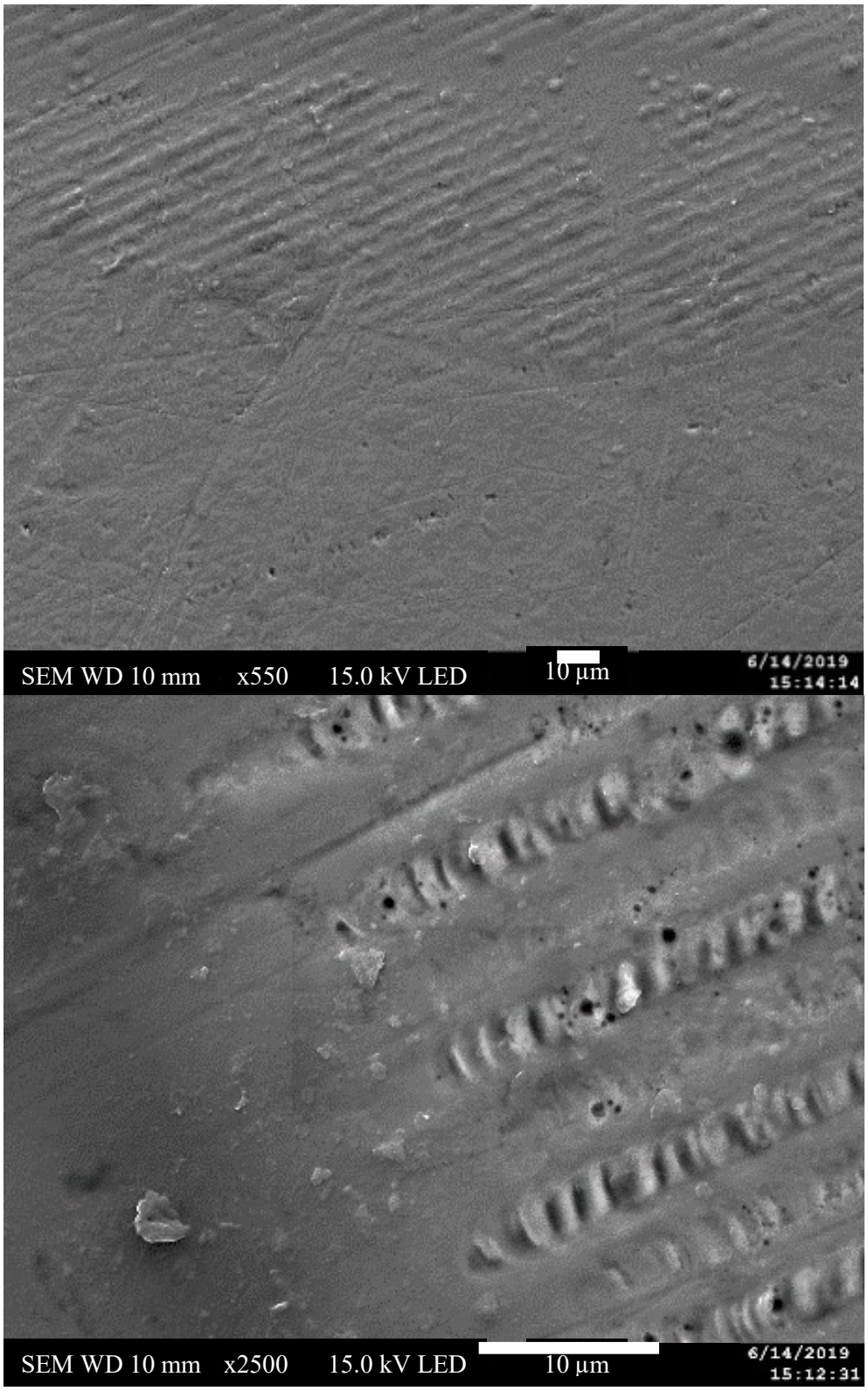

Figure A6: Cut and polished MnO-doped zinc borosilicate glass, of Mn/Zn ratio 0.015:1, post femtosecond laser irradiation of 0.5 mm/s rastering speed and ≈ 7.8 W, examined via backscattering electron SEM and exhibiting thin film scribing.

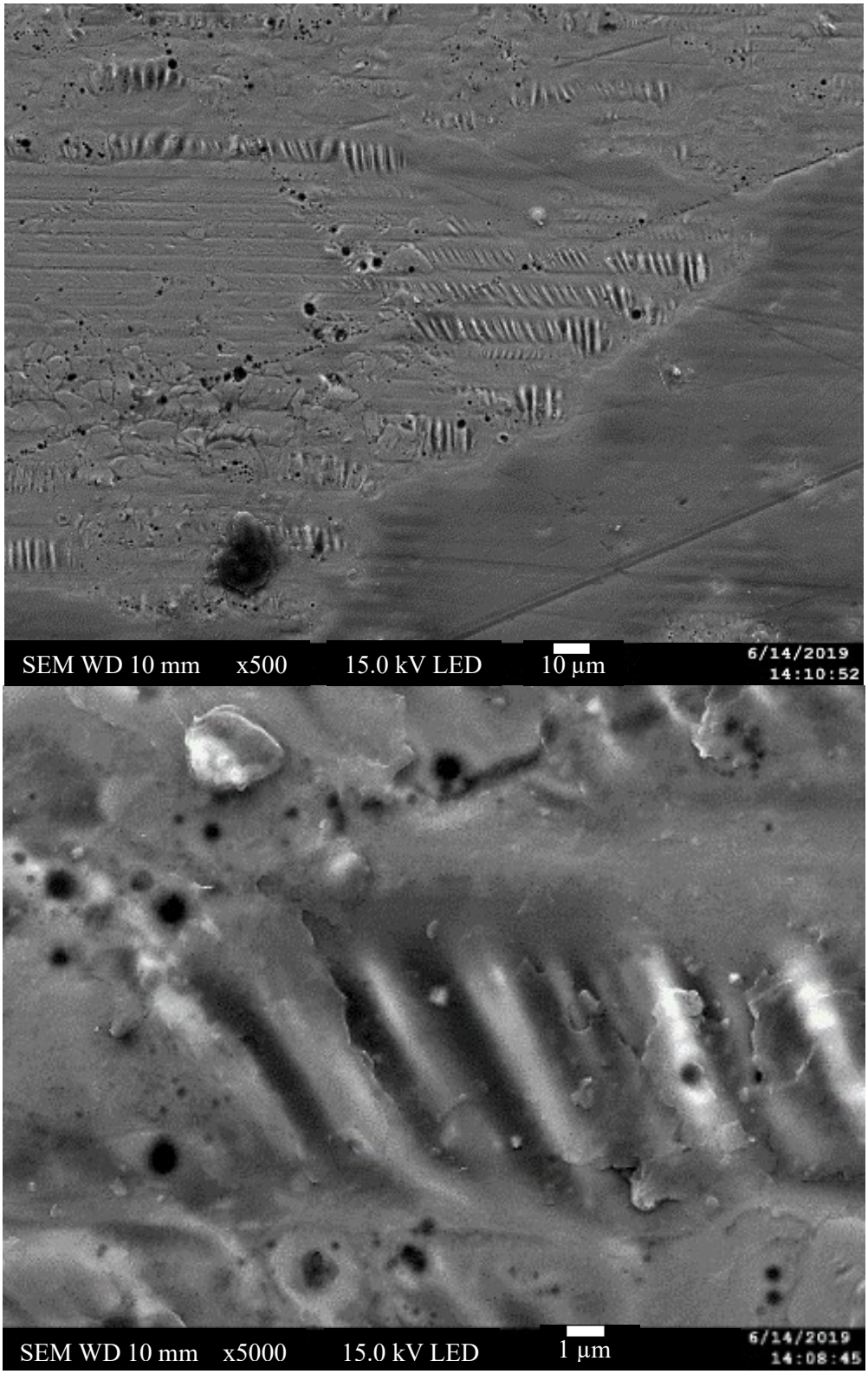

Figure A7: Cut and polished zinc borosilicate glass, post femtosecond laser irradiation of 0.5 mm/s rastering speed and ≈ 7.8 W, examined via backscattering electron SEM and exhibiting either thin film scribing or ultrafast annealing.

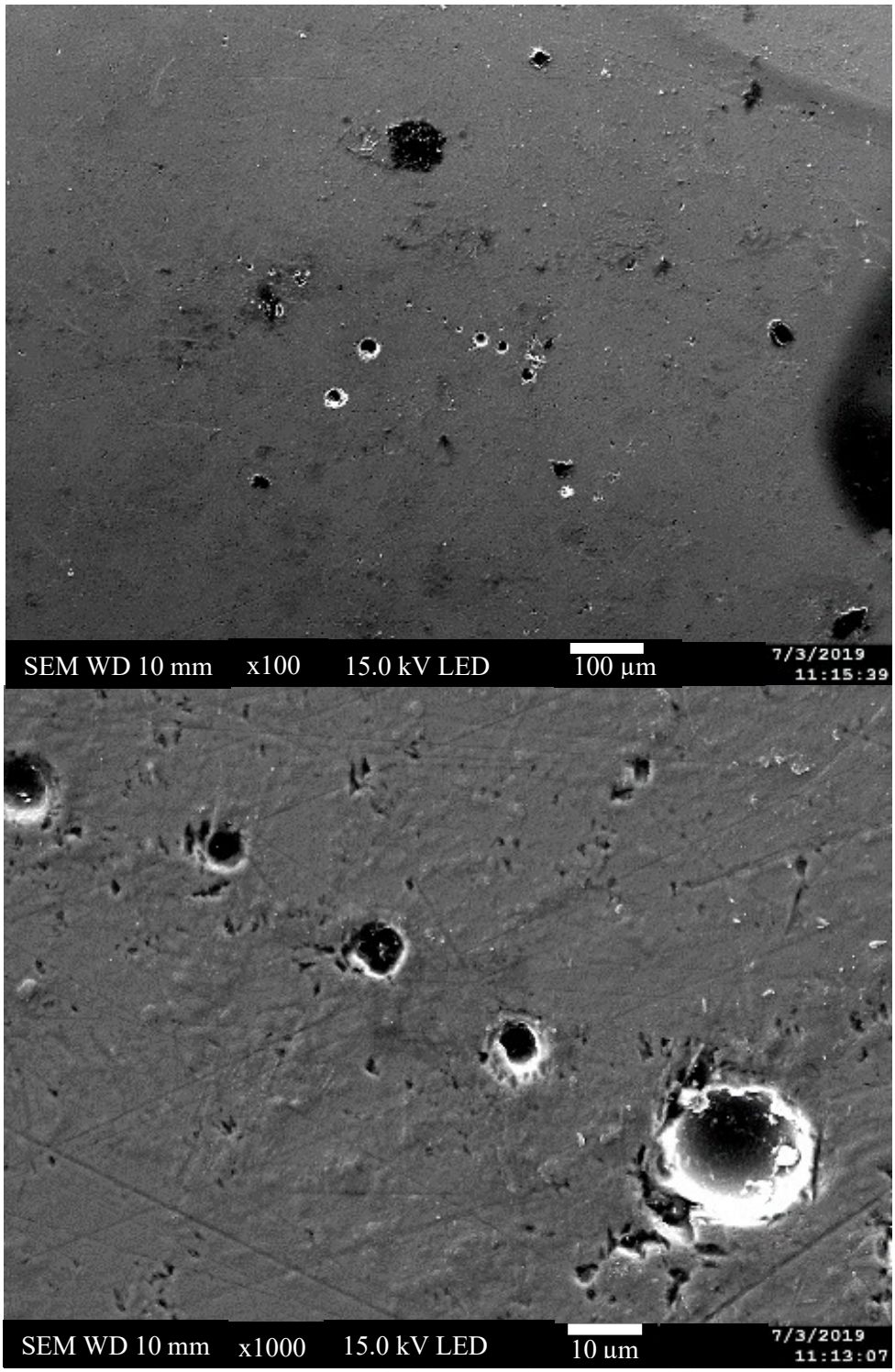

Figure A8: Cut and polished MnO-doped zinc borosilicate glass, of Mn/Zn ratio 0.01:1, post femtosecond laser radiation of 1 mm/s rastering speed and ≈ 7.8 W, examined via backscattering electron SEM and exhibiting structures similar to ns ablation.

The final structure that was observed in the treated samples was a small array of nanowire forming at and near surface of undoped zinc borosilicate glass as seen in Figure A9 below. It is unclear if this structure consistently appeared within the samples as it was only observed at one location of the examined samples. It is also unclear if the nanowire was formed via femtolaser interaction, the lack of notable ablation or other laser-surface interactions indicate that this may have been a formation within the glass prior to laser irradiation. It is known, however, that there are examples of ZnO and other crystalline nanowire structures being produced via femtosecond laser irradiation in studies done by other research groups.[18] Due to the size of the structure, it was not possible to use EDS to determine its atomic make up, instead the general phase the structure is forming was detected to be primarily oxygen and silicon, 34% and 32% respectively, with a comparatively moderate 15% zinc content. Due to the limited amount of information and the lack of high-resolution surface phase identification, it is difficult to determine whether the nanofibers are SiO_2, ZnO, or boron-based crystallites. The amount of zinc oxide initially added to the glass composition and the fact that some early attempts at sample creation lead to phase separation into borate striations suggests that this crystallite formation is most likely either zinc oxide or borate.

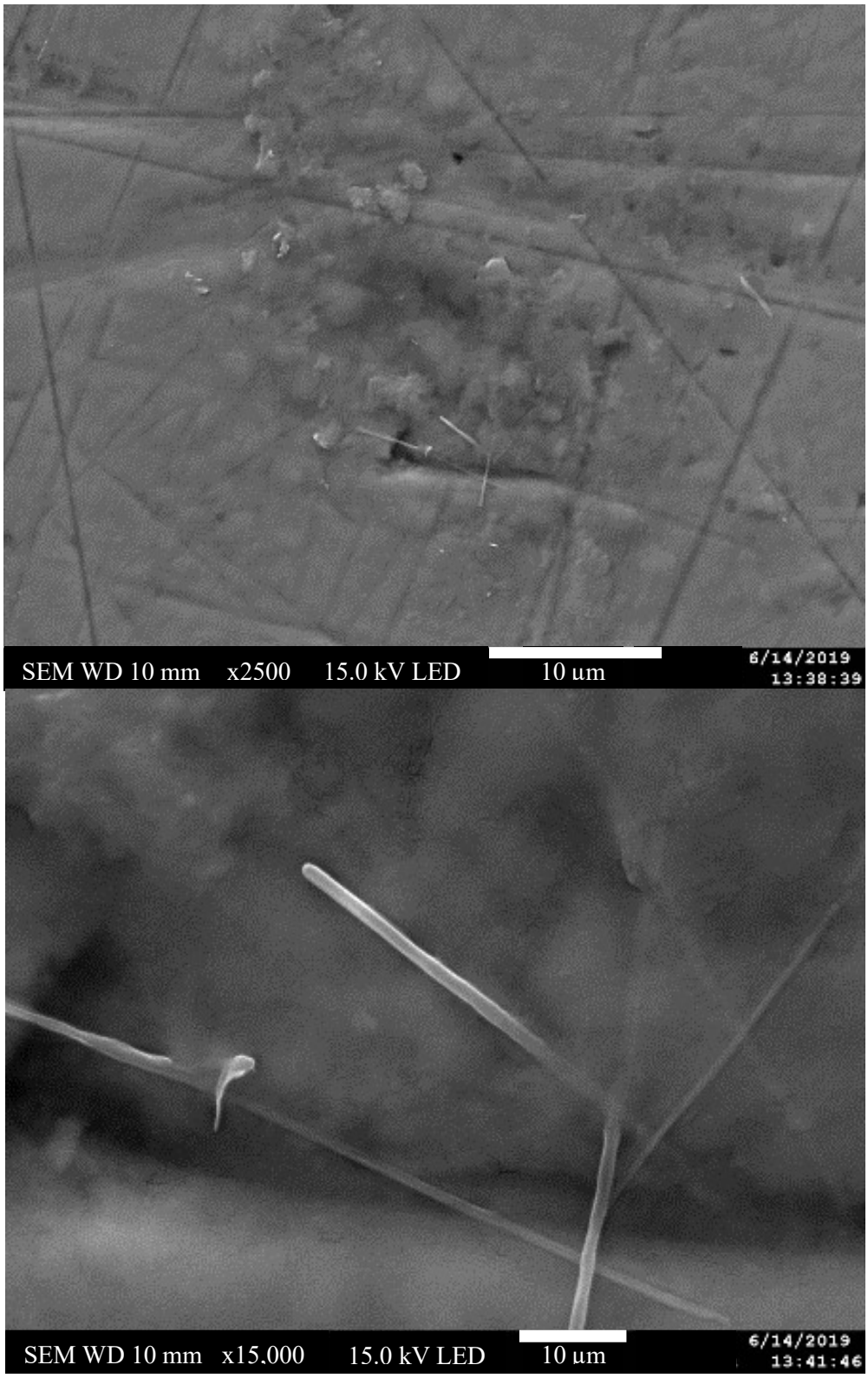

Figure A9: Cut and polished zinc borosilicate glass, post femtosecond laser irradiation of 1 mm/s rastering speed and ≈ 7.8 W, examined via backscattering electron SEM and exhibiting ZnO nanowire, potentially Mn doped, in a silicate phase.

C. Raman Spectroscopy

Raman spectroscopy, using low-intensity laser to avoid fluorescing the Mn within the compositions, was performed on the treated and untreated samples, however, minimal if any consistent change in peak intensity or location was observed.

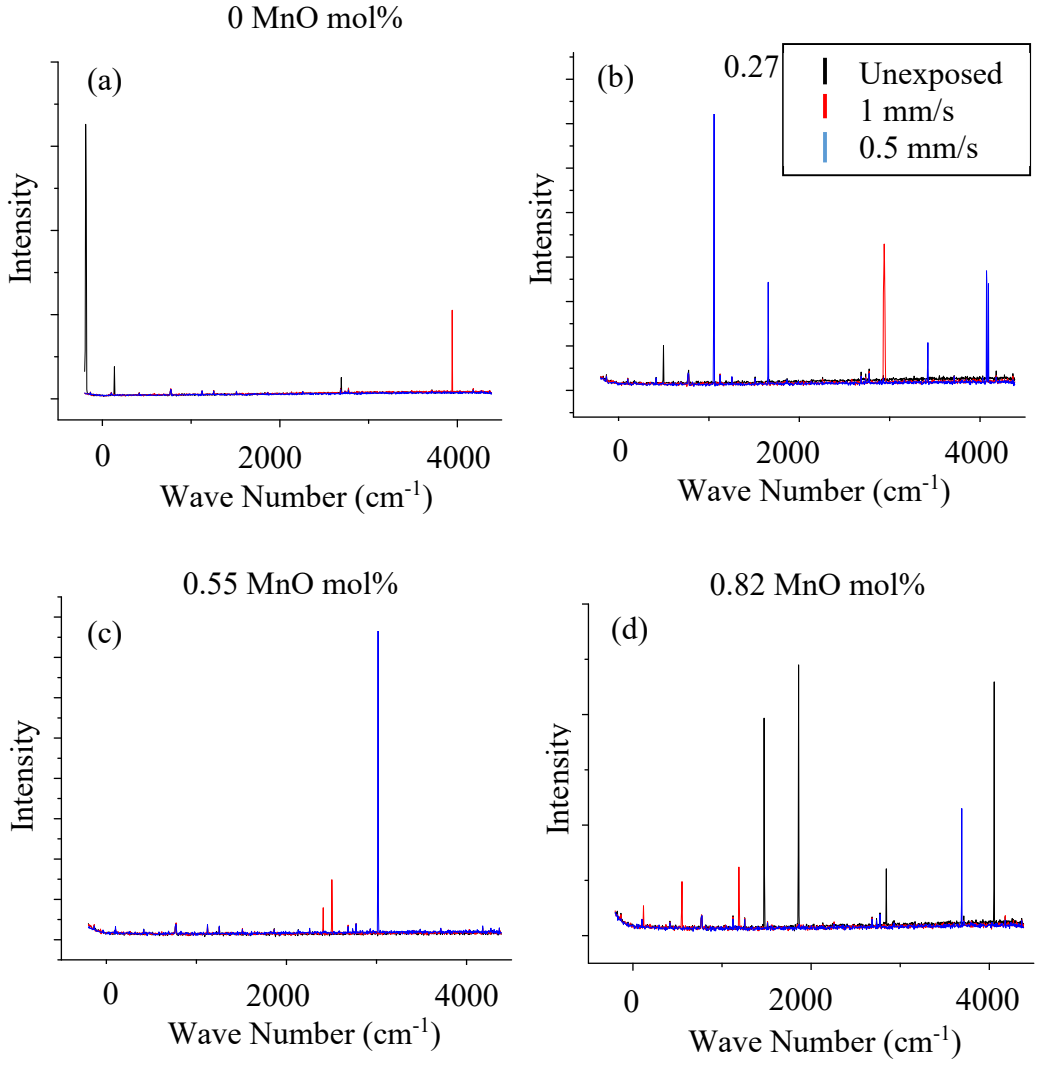

Figure A10: Raman peaks of MnO-doped zinc borosilicate glass, of Mn/Zn ratios 0, 0.005, 0.01, and 0.015 for compositions of MnO mol% 0 – 0.82 respectively (a-d) exhibiting the effects of laser irradiation at rastering speeds 1mm/s and 0.5 mm/s.

D. Terahertz Time Domain Spectroscopy

The refractive index (RI) and absorbance of MnO-doped zinc borosilicate glass, of Mn/Zn ratios 0, 0.005, 0.01, and 0.015 for compositions of MnO mol% 0 – 0.82 respectively, was observed untreated and after the irradiation with femtolaser laser at rastering speed 1mm/sec and 0.5 mm/s, as seen in Figure A11 via THz time-domain spectroscopy (THz-TDS). This was performed identifying any minute changes that might be found in optical or electrical properties in THz frequencies due to laser irradiation altering the local structure of the glass. The longer THz wavelength could potentially reflect stability issues in the glass caused by laser irradiation. It was found that for both RI and absorbance, the effects of Mn dopant are either negligible or decrease at low concentrations, as MnO-doped zinc borosilicate glass, of Mn/Zn ratio 0.005, was rather similar to zinc borosilicate glass, but MnO-doped zinc borosilicate glass, of Mn/Zn ratios 0.01, was less than both glass of Mn:Zn ratio 0 or 0.005 for both RI and absorbance. Only once the Mn content reaches the 0.015 Mn:Zn ratio did there occur a consistent increase in both RI and absorbance. The 0.5 mm/s rastering speed caused the RI to be generally less than the untreated version, but with exceptions at some THz. These results show that irradiation of femtosecond laser pulse appeares to have no consistent effect on the absorbance of the samples.

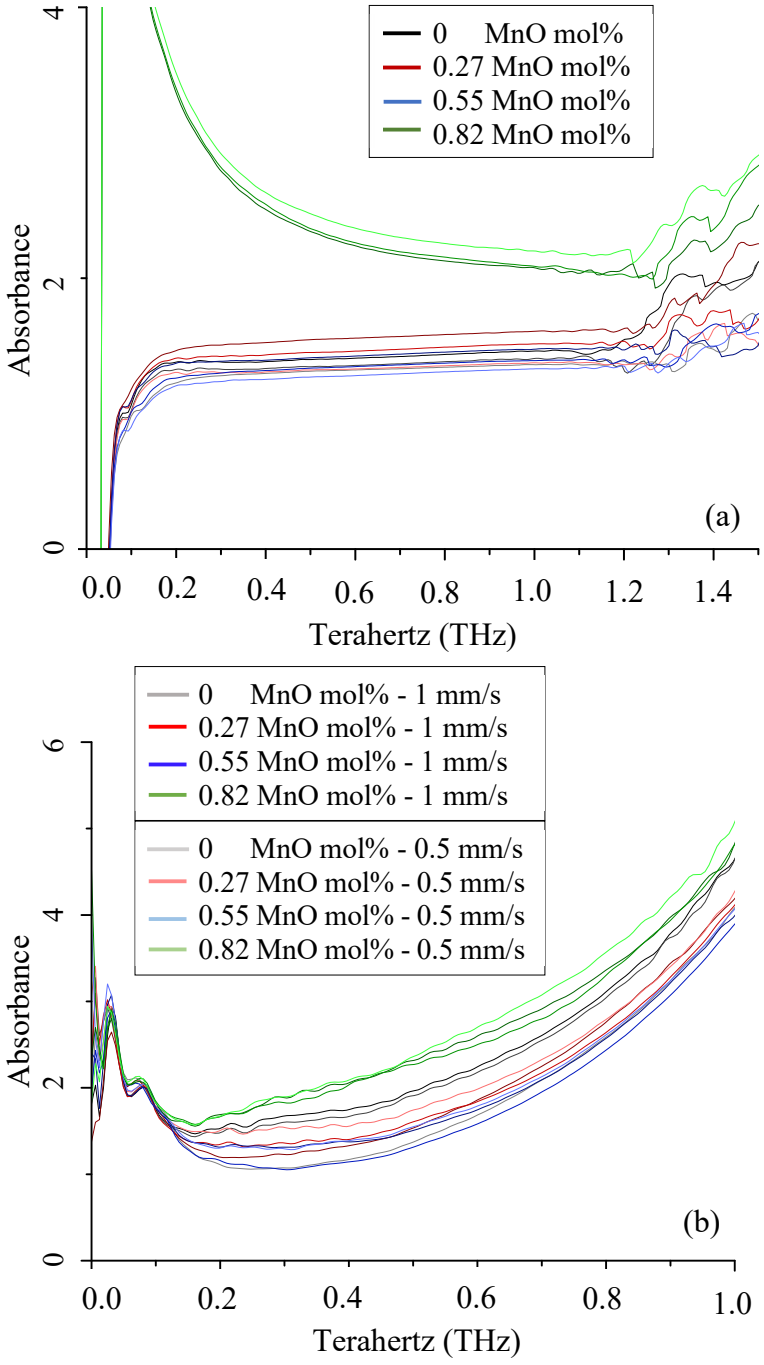

Figure A11: Refractive Index(a) and Absorbance(b) peaks of MnO-doped zinc borosilicate glass powder, of Mn/Zn ratios 0, 0.005, 0.01, and 0.015 for compositions of MnO mol% 0 – 0.82 respectively.

Figure A12 shows the THz optical properties at 0.8 THz. The results exhibit an increase in absorbance with decreasing rastering speed for MnO-doped zinc borosilicate glass, of Mn/Zn ratio 0.015, while for Mn:Zn ratios 0, 0.005, and 0.01 a decrease in absorbance is observed with decreasing rastering speed as seen in Figure A13(b). There appears to be little correlation between MnO content and the rate of decreasing absorbance with rastering speed for glass with Mn:Zn ratios 0, 0.005, and 0.01. The behavior of glass with Mn:Zn ratio 0.015, however, could potentially be caused by the formation of manganese zinc silicate, or due to the Zn displaced by the Mn into either zinc borate or some other position, being slightly more receptive to laser irradiation causing modification that increases THz absorbance.

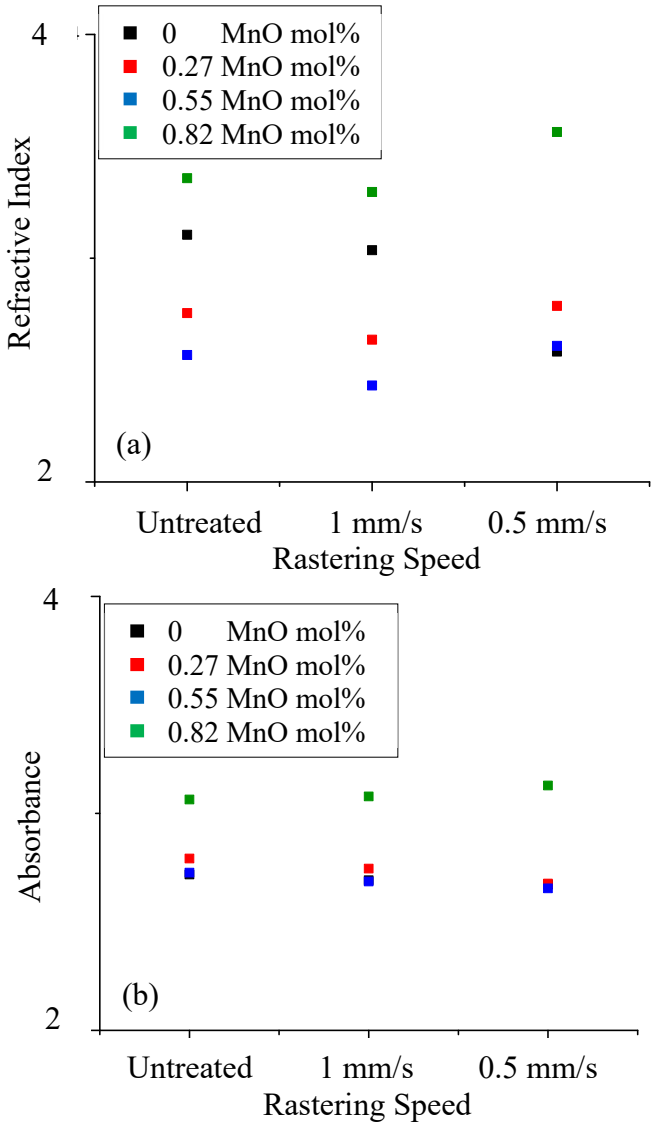

Figure A12: 0.8 THz Comparison RI (a) and Absorbance (b) of MnO-doped zinc borosilicate glass powder, of Mn/Zn ratios 0, 0.005, 0.01, and 0.015 for compositions of MnO mol% 0 – 0.82 respectively.

E. Additional THz Data Generated

Refractive Index

The refractive index of the compositions at varying rastering speeds and untreated by laser application at 0.8 THz in Figure A13(a) exhibits one interesting occurrence wherein the laser irradiation at 1 mm/s consistently affects all samples, decreasing the RI, but 0.5 mm/s rastering speed does not show such a consistent effect. The 0.5 mm/s rastering speed shows an increase in RI for all compositions containing Mn, while zinc borosilicate glass, containing no Mn, has a comparatively sharp decrease in RI. The increase in RI, when comparing 0.5 mm/s rastering speed of laser irradiation to 1 mm/sec or untreated, does have a positive correlation with increasing Mn content.

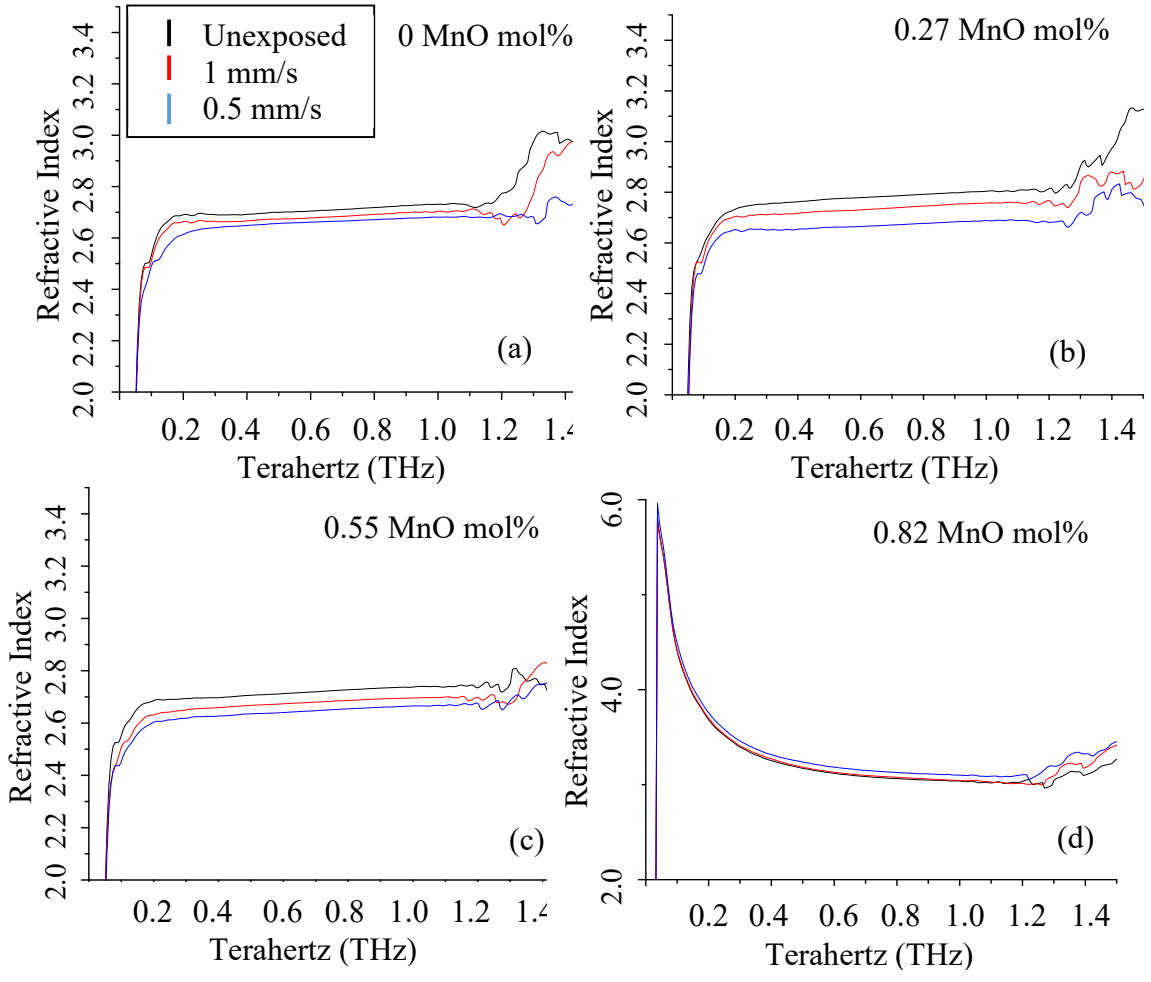

Figure A13: Refractive index of MnO-doped zinc borosilicate glass, of Mn/Zn ratios 0, 0.005, 0.01, and 0.015 for compositions of MnO mol% 0 – 0.82 respectively (a-d) measured via THz Time-Domain.

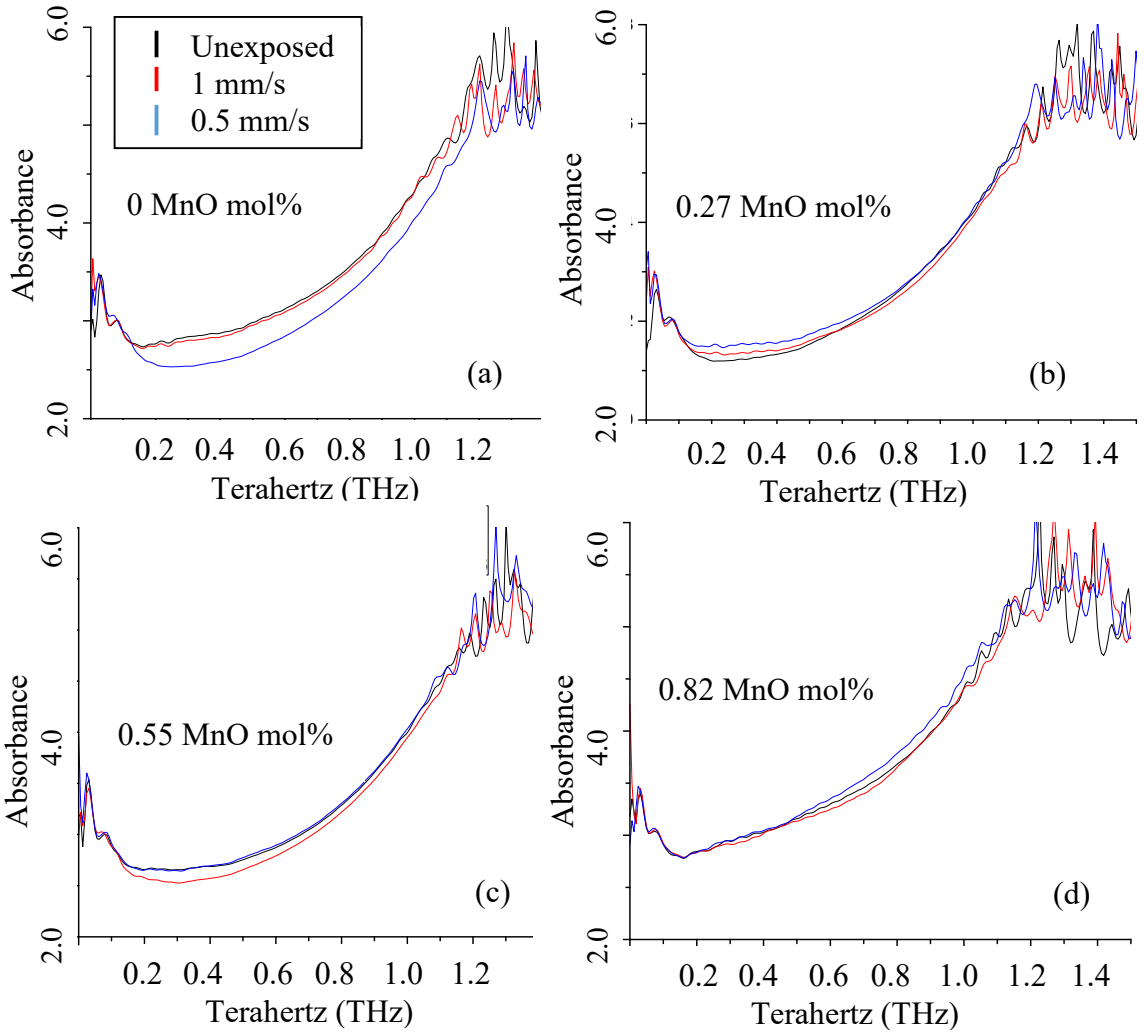

Figure A14: Absorbance of MnO-doped zinc borosilicate glass, of Mn/Zn ratios 0, 0.005, 0.01, and 0.015 for compositions of MnO mol% 0 – 0.82 respectively (a-d) measured via THz Time-Domain.

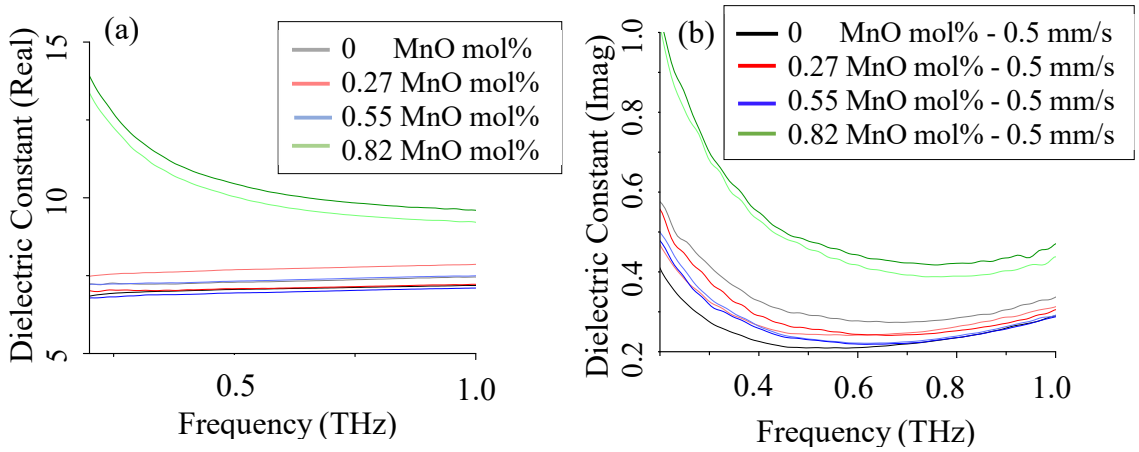

Figure A15: Dielectric Relative Permittivity Real(a) and Imaginary(b) of MnO-doped zinc borosilicate glass, of Mn/Zn ratios 0, 0.005, 0.01, and 0.015 for compositions of MnO mol% 0 – 0.82 respectively.

F. DSC-TGA Data

1. Temperature Difference

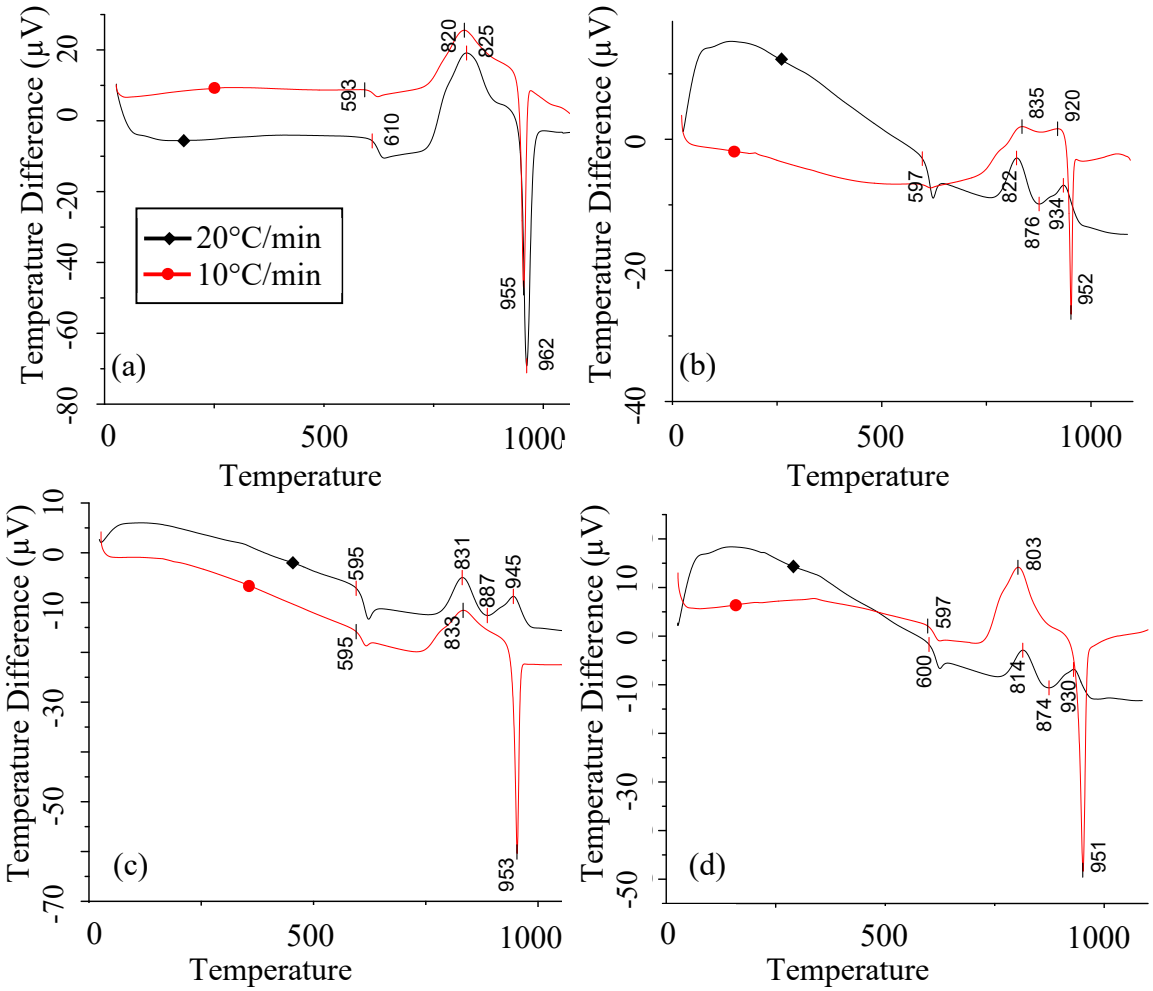

Figure A16: Exo- and endothermic temperature difference of MnO-doped zinc borosilicate glass, of Mn/Zn ratios 0, 0.005, 0.01, and 0.015 for compositions of MnO mol% 0 – 0.82 respectively (a-d) vs temperature, measured via differential scanning calorimetry. Samples were measured at a 20°C/min heating-rate and a 10°C/min heating-rate.

G. XRD Spectropscopy Data

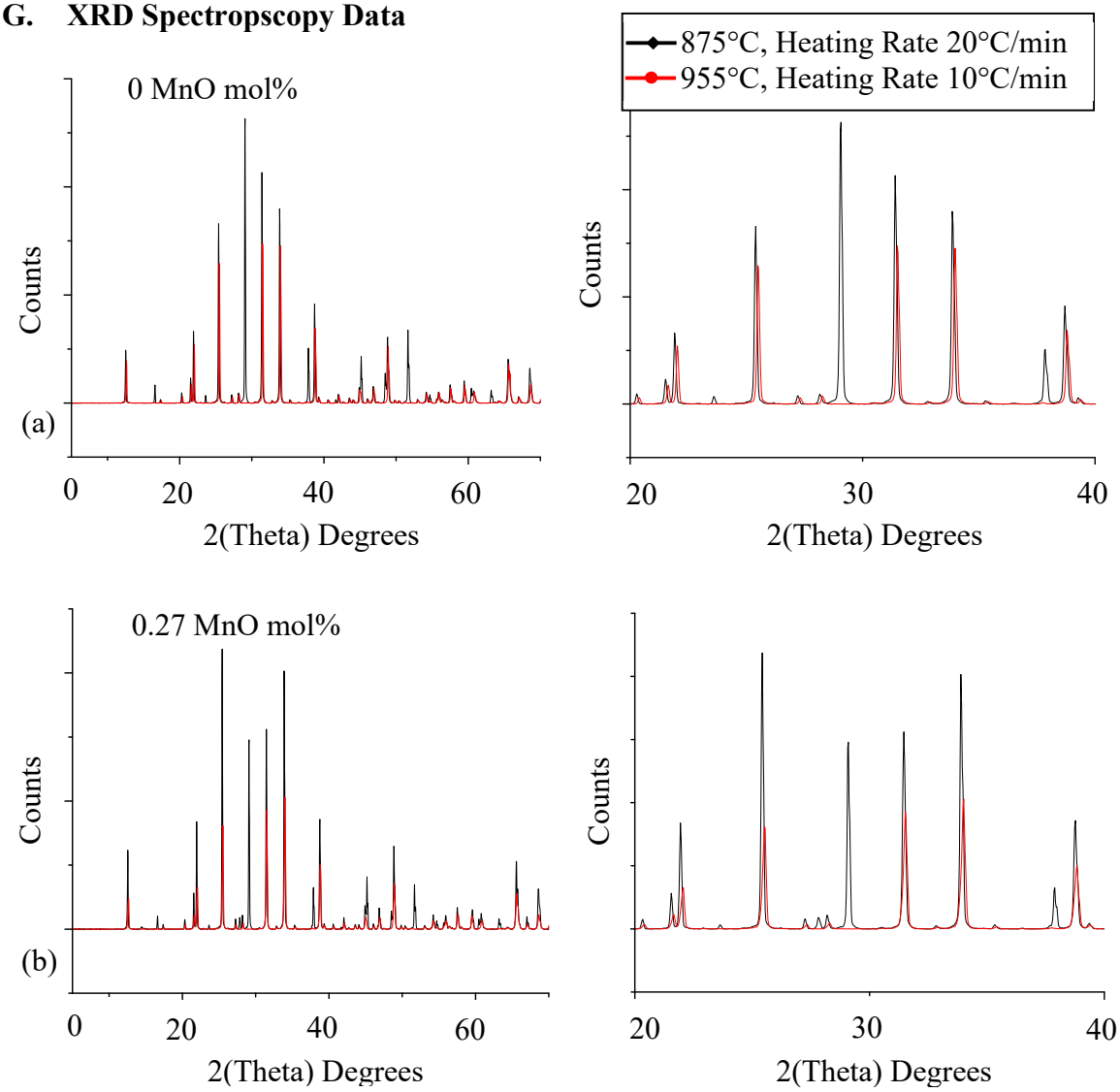

Figure A17: XRD peaks of MnO-doped zinc borosilicate glass powder, of Mn/Zn ratios 0(a) and 0.005(b), of compositions MnO mol% 0 and 0.27 respectively, comparison between heat-treatment to 875°C at a rate of 20°C/min and to ≈ 955°C/min at a rate of 10°C/min.

H. SEM and EDS Data

Spot Analysis

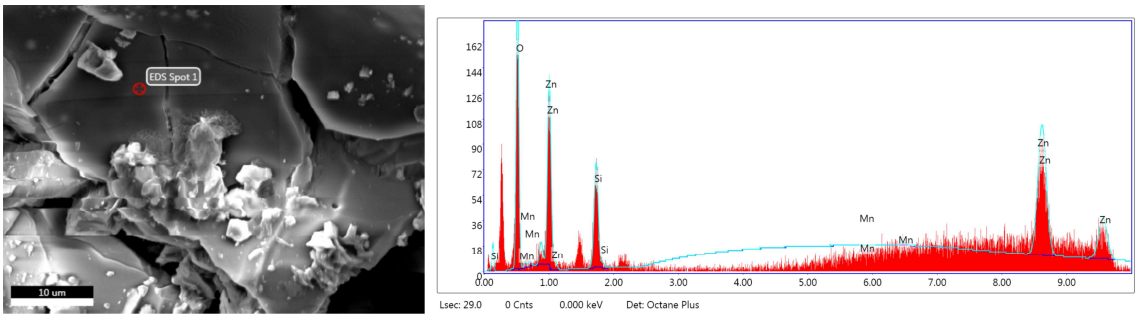

Figure A18, Table AI: Energy Dispersive Spectroscopy based elemental spot analysis of MnO-doped zinc borosilicate glass powder, of Mn/Zn ratio 0.005:1; location 2, spot 1, post heat-treatment at 875°C.

Element	Weight %	Atomic %	Net Int.	Error %	K ratio	Z	A	F
O K	10.57	31.45	70.75	10.13	0.0502	1.2844	0.3696	1.000
SiK	3.53	5.98	39.17	11.46	0.0201	1.1696	0.4863	1.001
MnK	0.06	0.05	0.27	69.02	0.0007	0.9749	0.9877	1.114
ZnK	85.84	62.52	104.21	8.08	0.8155	0.9472	1.0011	1.001

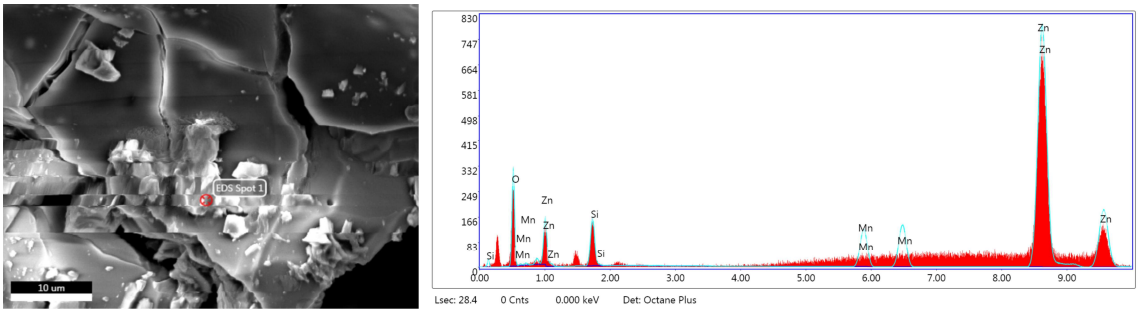

Figure A19, Table AII: Energy Dispersive Spectroscopy based elemental spot analysis of MnO-doped zinc borosilicate glass powder, of Mn/Zn ratio 0.005:1; location 2, spot 2, post heat-treatment at 875°C.

Element	Weight %	Atomic %	Net Int.	Error %	K ratio	Z	A	F
O K	2.07	7.82	116.41	9.81	0.0097	1.3281	0.3524	1.000
SiK	0.98	2.11	91.13	9.74	0.0055	1.2102	0.4607	1.001
MnK	3.11	3.42	119.58	4.29	0.0342	1.0120	0.9854	1.101
ZnK	93.84	86.65	1008.20	3.87	0.9263	0.9875	0.9990	1.000

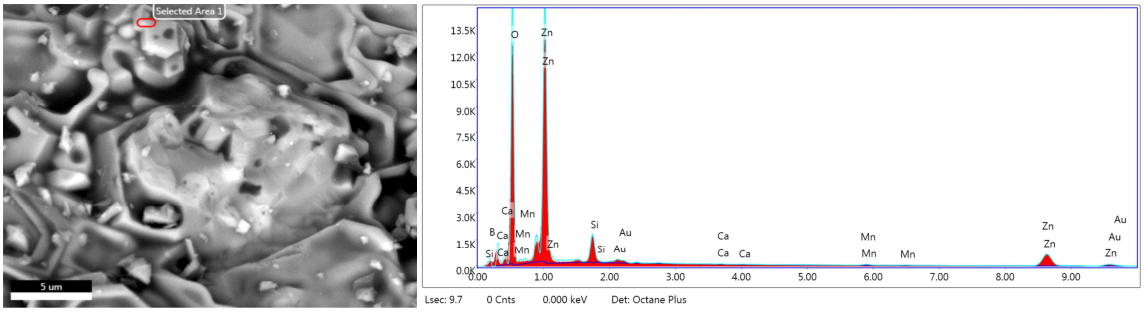

Figure A20, Table AIII: Energy Dispersive Spectroscopy based elemental spot analysis of MnO-doped zinc borosilicate glass powder, of Mn/Zn ratio 0.01:1; location 3, spot 1, post heat-treatment at 875°C.

Element	Weight %	Atomic %	Net Int.	Error %	K ratio	Z	A	F
B K	27.72	47.25	454.26	11.24	0.0525	1.0915	0.1735	1.0000
O K	36.09	41.58	16440.94	7.46	0.1599	1.0932	0.4051	1.0000
SiK	2.90	1.90	2816.60	5.77	0.0198	0.9886	0.6893	1.0018
AuM	0.81	0.08	302.05	17.57	0.0061	0.6224	1.1935	1.0088
CaK	0.07	0.03	42.62	59.43	0.0007	0.9295	0.9745	1.0155
MnK	0.53	0.18	140.99	28.10	0.0047	0.8112	1.0052	1.0823
ZnK	31.87	8.99	2360.71	4.90	0.2527	0.7742	1.0066	1.0171

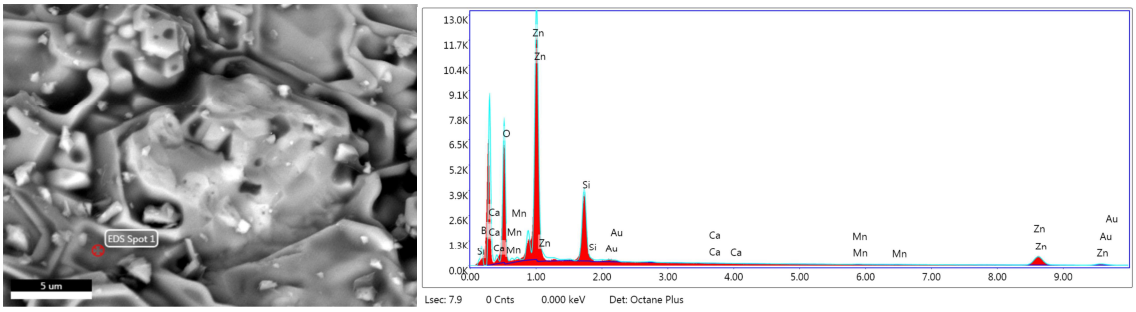

Figure A21, Table AIV: Energy Dispersive Spectroscopy based elemental spot analysis of MnO-doped zinc borosilicate glass powder, of Mn/Zn ratio 0.01:1; location 3, lower left spot 1, post heat-treatment at 875°C.

Element	Weight %	Atomic %	Net Int.	Error %	K ratio	Z	A	F
B K	48.98	69.69	1060.92	10.49	0.1021	1.0625	0.1963	1.0000
O K	22.66	21.79	9640.29	8.51	0.0781	1.0618	0.3247	1.0000
SiK	6.12	3.35	7810.38	4.26	0.0457	0.9579	0.7782	1.0020
AuM	0.47	0.04	211.46	23.55	0.0035	0.6028	1.2497	1.0082
CaK	0.03	0.01	17.96	72.56	0.0002	0.8993	0.9884	1.0183
MnK	0.16	0.04	48.94	59.79	0.0014	0.7837	1.0089	1.0959
ZnK	21.59	5.08	1868.65	5.51	0.1666	0.7462	1.0069	1.0271

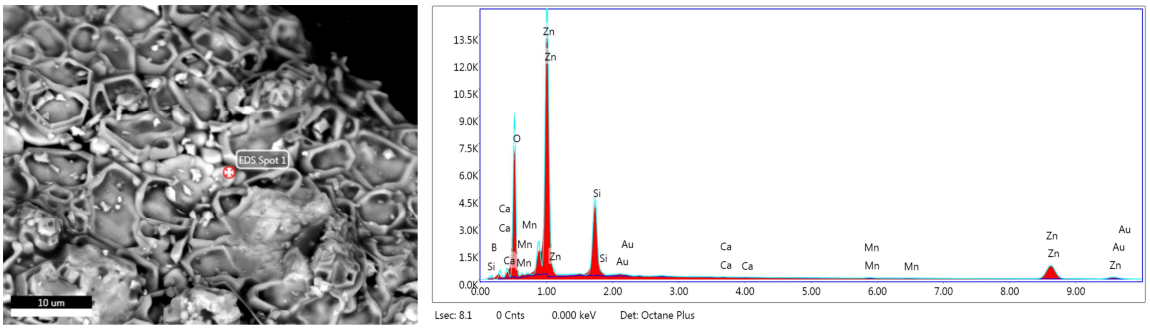

Figure A22, Table AV: Energy Dispersive Spectroscopy based elemental spot analysis of MnO-doped zinc borosilicate glass powder, of Mn/Zn ratio 0.01:1; location 3,upper right spot 1, post heat-treatment at 875°C.

Element	Weight %	Atomic %	Net Int.	Error %	K ratio	Z	A	F
B K	18.10	37.84	204.40	13.30	0.0260	1.1334	0.1265	1.000
O K	27.43	38.76	11243.25	7.76	0.1201	1.1375	0.3849	1.000
SiK	10.08	8.12	8638.04	5.48	0.0666	1.0309	0.6398	1.001
AuM	0.51	0.06	165.33	27.60	0.0037	0.6494	1.1001	1.008
CaK	0.08	0.05	43.38	60.87	0.0008	0.9708	0.9522	1.017
MnK	0.44	0.18	110.61	38.94	0.0040	0.8488	0.9991	1.091
ZnK	43.36	14.99	3048.63	4.67	0.3585	0.8129	1.0048	1.012

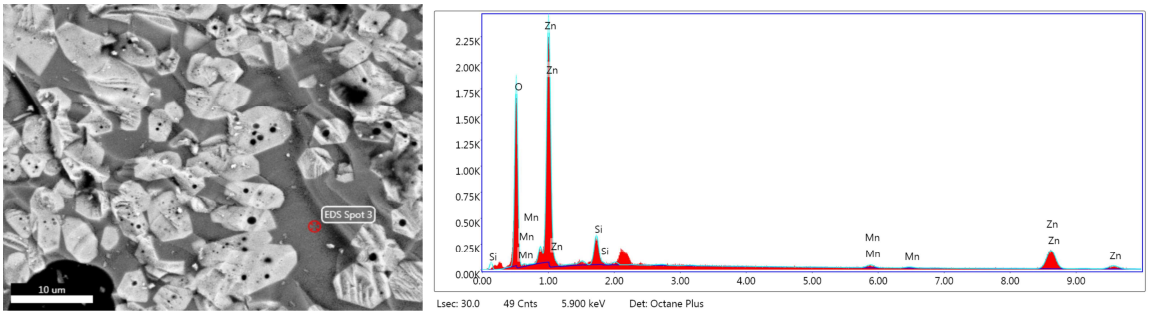

Figure A23, Table AVI: Energy Dispersive Spectroscopy based elemental spot analysis of MnO-doped zinc borosilicate glass powder, of Mn/Zn ratio 0.015:1; location 2, spot 3, post heat-treatment at 951°C with a ramp rate of 10°C/min.

Element	Weight %	Atomic %	Net Int.	Error %	K ratio	Z	A	F
O K	32.83	64.50	756.14	7.52	0.1754	1.1932	0.4477	1.000
SiK	4.73	5.29	170.16	9.09	0.0284	1.0841	0.5536	1.001
MnK	2.05	1.18	25.61	28.33	0.0203	0.8970	0.9951	1.105
ZnK	60.39	29.04	206.91	6.07	0.5268	0.8638	1.0028	1.007

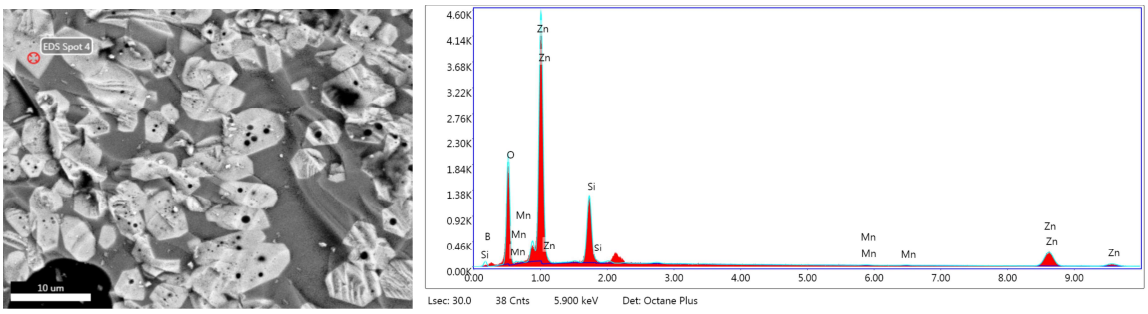

Figure A24, Table AVII: Energy Dispersive Spectroscopy based elemental spot analysis of MnO-doped zinc borosilicate glass powder, of Mn/Zn ratio 0.015:1; location 2, spot 4, post heat-treatment at 951°C with a ramp rate of 10°C/min.

Element	Weight %	Atomic %	Net Int.	Error %	K ratio	Z	A	F
B K	27.54	52.21	32.30	13.85	0.0425	1.1217	0.1374	1.000
O K	22.34	28.61	812.06	8.39	0.0895	1.1251	0.3561	1.000
SiK	8.29	6.05	697.14	5.90	0.0554	1.0190	0.6545	1.001
MnK	0.27	0.10	6.65	61.27	0.0025	0.8381	1.0014	1.118
ZnK	41.56	13.03	280.38	5.57	0.3393	0.8017	1.0054	1.012

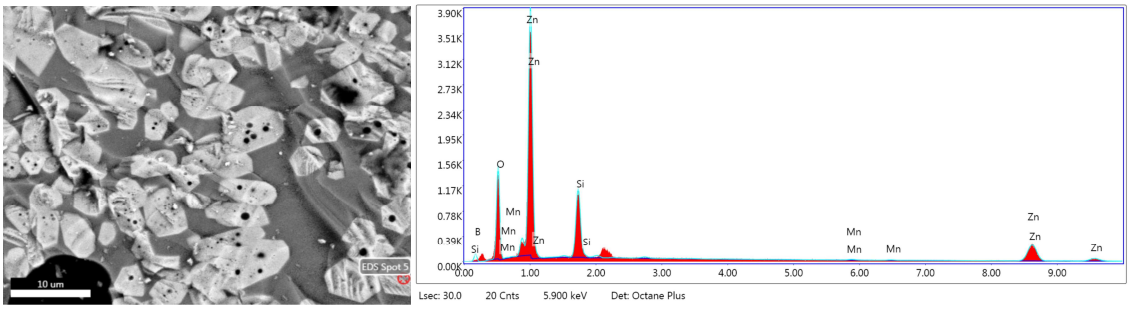

Figure A25, Table AVIII: Energy Dispersive Spectroscopy based elemental spot analysis of MnO-doped zinc borosilicate glass powder, of Mn/Zn ratio 0.015:1; location 2, spot 5, post heat-treatment at 951°C with a ramp rate of 10°C/min.

Element	Weight %	Atomic %	Net Int.	Error %	Kratio	Z	A	F
B K	32.12	59.60	37.55	13.41	0.0511	1.1240	0.1416	1.0000
O K	17.43	21.85	580.13	8.80	0.0662	1.1274	0.3370	1.0000
SiK	7.48	5.34	608.49	5.98	0.0500	1.0212	0.6543	1.0016
MnK	0.41	0.15	9.87	60.24	0.0038	0.8401	1.0016	1.1179
ZnK	42.56	13.06	277.77	5.54	0.3481	0.8037	1.0056	1.0118

Additional Images

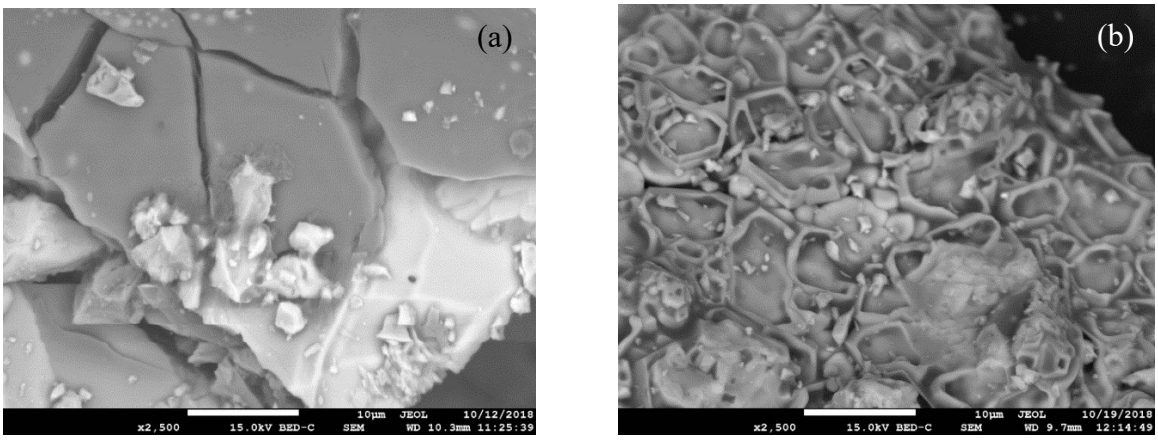

Figure A26: Scanning electron microscopic imaging of MnO-doped zinc borosilicate glass powder, of Mn/Zn ratios 0.005:1(a) and 0.01:1(b) of compositions MnO mol% 0.27 and 0.55 respectively after heat-treatment at 875°C.

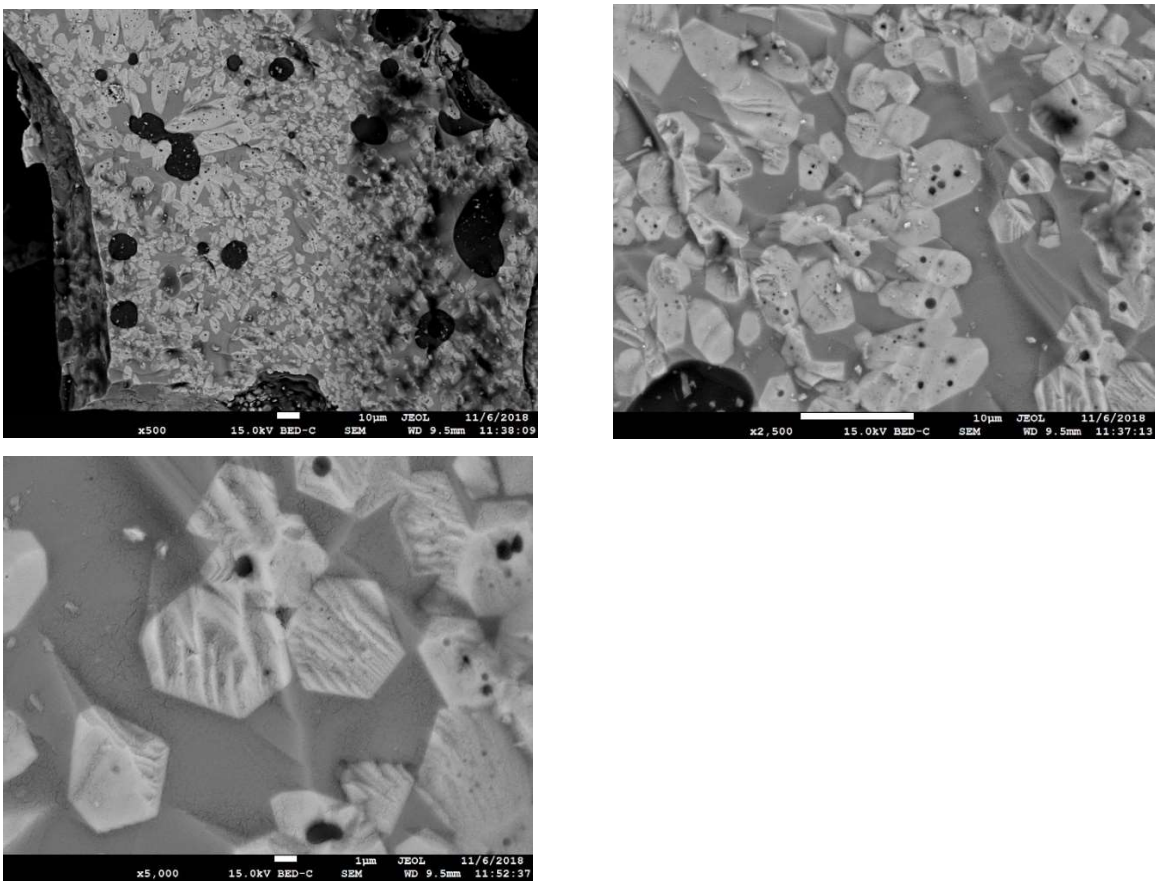

Figure A27: SEM imaging of Energy Dispersive Spectroscopy based elemental spot analysis of MnO-doped zinc borosilicate glass powder, of Mn/Zn ratio 0.015:1 of composition MnO mol% 0.82 after heat-treatment at 951° C with a ramp rate of 10°C/min.

VII. REFERENCES

1. Hamilton, E. H., et al., Properties of zinc borosilicate glasses; *Journal of Research of the National Bureau of Standards*, **62**(2) pp. 59-62 (1959).

2. Kupracz, P., et al., Microstructure and electrical properties of manganese borosilicate glasses*; Journal of Non-Crystalline Solids*, **423-424** pp. 68-75 (2015).

3. Chen, G., et al., Photoluminescent properties of nanocrystallized zinc borosilicate glasses; *Radiation Measurements*, **38**(4) pp. 771-774. Department of Inorganic Materials, East China University of Science and Technology, Shanghi, China, (2004).

4. Kullberg, A. T. G., et al. Formation and crystallization of zinc borosilicate glasses: Influence of the ZnO/B_2O_3 ratio; *Journal of Non-Crystalline Solids*, **441** pp. 79-85 (2016).

5. Kullberg, A. T. G., et al., Crystal growth in zinc borosilicate glasses; *Journal of Crystal Growth*, **457** pp. 239-243 (2017).

6. Ehrt, D., Zinc and manganese borate glasses - Phase separation, crystallisation, photoluminescence and structure; *Glass Science Technology Journal* **54**(2), pp. 65-75, Otto-Schott Institute, Friedrich-Schiller University, Jena, Germany (2013).

7. Keskenler, E. F., et al., Evaluation of Structural and Optical Properties of Mn-Doped ZnO Thin Films Synthesized by Sol-Gel Technique; *Metallurgical and Materials Transactions*, **43**(13) pp. 5088-5095 (2012).

8. Kupracz, P., et al., Polaron hopping conduction in manganese borosilicate glass; *Journal of Non-Crystalline Solids*, **458** pp. 15-21 (2017).

9. Li, C., et al., Multi-color long-lasting phosphorescence in Mn^{2+}-doped $ZnO–B_2O_3–SiO_2$ glass–ceramics; *Materials Research Bulletin*, **37**(8) pp. 1443-1449 (2002).

10. Krol, D. M., Femtosecond laser modification of glass; *Journal of Non-Crystalline Solids,* **354**(2) pp. 416-424 (2008).

11. Seuthe, T., et al., Structural relaxation phenomena in silicate glasses modified by irradiation with femtosecond laser pulses; *Scientific Reports*, **7** pp. 43815 (2017).

12. Kongsuwan, P., Laser Induced Modification and Integration of Glasses; *The Graduate School of Arts and Sciences, Columbia University. Doctor of Philosophy*, pp. 209 (2014).

13. Dixon, *K. M.*, Femtosecond Laser Modification of $ZnO-B_2O_3-SiO_2$ Glasses; *N.Y.S. College of Ceramics. Alfred, New York, Alfred University. Bachelor of Science* (2017).

14. Self, Katherine et al., Reversed Crystal Growth of ZnO Microdisks; *Chemical communications, Cambridge,* **49**(47) pp. 5411-5413 (2013).

15. Iraj Kazeminezhad, Ramin Yousefi., Growth and characterization of ZnO (microdisks)/$W_{18}O_{49}$ (nanorods) heterostructures; *Solid State Sciences*, **14** pp. 349-353 (2012)

16. Terol, S & J., Otero, Maria., Anhydrous Zinc Borate as a Host Crystal in Luminescence. *Zeitschrift Fur Naturforschung Section A-a Journal of Physical Sciences*, **16** pp. 1961-0915 (1961).

17. Phillips K. et al., Ultrafast laser processing of materials: a review; *Advances in Optics and Photonics*, 7(4) pp. 684-712 (2015).

18. Baba, M., Jia, T., Suzuki, M., & Kuroda, H.. Femtosecond laser induced nanowire technique and its applications; *ISRN Nanotechnology,* (2011)

19. Carolyn Jones Otten, Oleg R. Lourie, Min-Feng Yu, John M. Cowley, Mark J. Dyer, Rodney S. Ruoff, and William E. Buhro1., Crystalline Boron Nanowires; *Journal of the American Chemical Society*, 124 (17) pp. 4564-4565 (2002).

20. Annam, R., et al., Fluorescence spectroscopic studies of Mn^{2+} ions in $SrO–Al_2O_3–B_2O_3–SiO_2$ glass system; *Optical Materials*, **35** pp. 402-406 (2013).

21. Kanehira, S., et al., Ion exchange in glass using femtosecond laser irradiation; *The American Institute of Physics*, **93**(2) pp. 023112 (2008).